Metabifurcation analysis of a phenomenological ventricular cell model

by

Wenyue Yang

A Thesis Submitted in Partial Fulfillment
of the Requirements for the Degree of

Master of Science

in

The Faculty of Science

Modelling and Computational Science

University of Ontario Institute of Technology

August 2018

Abstract

Heart disease is the leading cause of death in America, and arrhythmia is considered one of the most important precursors of heart attacks. We cannot predict arrhythmia directly; however, it has been shown that cardiac alternans is closely related to arrhythmia[35]. Therefore, predicting alternans could be the first step in preventing arrhythmia. Fenton and Karma(1998)[10] came up with the Fenton-Karma model (the F-K model) with three variables and 13 parameters that is a relatively simple and basic model that including information on alternans. Our research is based on the F-K model at the cell level rather than the tissue level.

We study the parameter space of the F-K model and discover robust correlations between parameters and dynamical responses. The relations cannot be disclosed by some statistical methods like principal component analysis(PCA) or K-means clustering because we cannot see the dynamical behaviors of parameter sets.

The links instead emerge when the parameter space is partitioned according to bifurcation responses. We call this general method "metabifurcation analysis". Concretely, the bifurcation responses are shown by the bifurcation plots, which show the model responses, like action potential duration(APD) restitution curves, to a sequential change in pacing frequency. According to the bifurcation patterns, we partition the parameter space in five "parent families". After investigating and characterizing them in depth, we subtly classify the largest parent families into four subfamilies. We discuss their essential differences in qualitative dynamical behaviors like whether they exhibit bistability and

how solutions change after alternans appears.

The partitioning cannot be achieved by the investigation of only a small number of parameter sets. To obtain a relatively large number of parameter sets to make the results reliable, we implement a particle swarm optimization process with parallel programming interfaces like OpenMP and Open MPI to search the parameter space and obtain 1,525,833 physiologically admissible parameter sets; then, we randomly choose a representative sample of 270,000 parameter sets to do the bifurcation analysis.

After doing the metabifurcation analysis on the the F-K model, some results are listed as follows. First, more than 70% parameter sets from 270,000 meaningful parameter sets do not or only have one period-doubling bifurcation. Second, τ_w^- plays the leading role of identifying subfamilies in the parent family(PF2) with only one period-doubling bifurcation; Moreover, in one subfamily(F3), there is a positive linear relation between τ_w^- and the appearance of bistability.

Acknowledgements

First, I would like to thank my supervisor Dr. Lennaert van Veen for his guidance and support throughout this project and Dr. Elizabeth M. Cherry, RIT, Rochester, U.S for providing the support. I would also like to thank the members and faculty of the Modelling and Computational Science program, particularly my fellow members of the C.L.A.I.M. Lab. Finally, I would like to thank my family and friends for their support and encouragement.

Contents

List of Tables

List of Figures

Chapter 1

Introduction

Myocardial infarction (MI)that is also known as a heart attack, causes the fatal damage to the heart muscle, and heart arrhythmia is the leading cause of MI.[33]

In a cardiac electrical system, an arrhythmia is a disturbance in the regular rhythm of heartbeats. When the rhythm is too fast, it is named tachycardia. If it is too slow, we call that bradycardia. Furthermore, it may be too early or irregular, we call them premature contraction and fibrillation separately. All these situations are caused by the problem of electrical signals that tell heart muscle the time to contract and relax. Because electrical impulses coordinating heartbeats are not working regularly, the heart beats too fast, too slowly or inconsistently. Some heart arrhythmias can be harmless; for example, everyone has experienced an irregular heartbeat at some time. However, some arrhythmias are detrimental to our health in some cases, which can be severe as to be potentially fatal; especially, rhythm varies extensively from a regular heartbeat. [21]

1.1 Cardiac Alternans

Cardiac alternans is defined as a condition that a periodic beat-to-beat oscillating electrical activity, and the strength of myofiber contraction varies between weak and strong rates rather than a constant heart rate.[8] Generally, alternans occurs at a high frequency
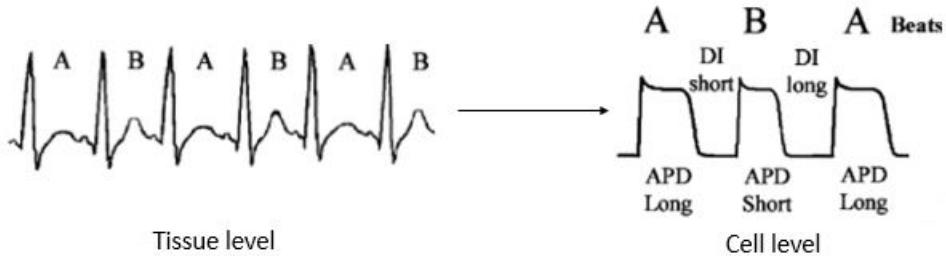
Figure 1.1: T wave alternans. The first graph is an electrocardiogram where "A" indicates a longer T wave, and "B" is a shorter T wave. The second graph is an electrical activity graph of a ventricular cell where "A" corresponds to a longer action potential(APD) restitution curve, and "B" correlates to a shorter APD restitution curve.[24]

of heartbeats, and it is typically related to increasing the risk of atrial and ventricular arrhythmia and sudden cardiac death.

Cardiac alternans is classified into mechanical alternans and electrical alternans; however, mechanical alternans occurs with electrical alternans. Electrical alternans can be observed in electrocardiogram as the alternation of T waves. Fig.1.1 displays the behavior of T-wave alternans at the single cell level and the tissue level. A longer T waves shown as "A", at the tissue level, corresponds to a longer action potential duration(APD) restitution curve and a shorter diastolic interval(DI) in the cell level; in contrast, a shorter T waves shown as "B" in the tissue level is corresponding to a shorter APD and a longer DI in the cell level. In both cases, cycle length(CL)=APD+DI where CL refers to the sequence of electrical events that repeats with each heartbeat.[19]

1.2 Cardiac Models

There are two different levels of cardiac models: cell-level models encoding information about excitability, and tissue-level models using electrical conduction to enable a quantitative description of action potential propagation.

Concerning the cardiac tissue models, there are two families: bidomain models consider cardiac tissue as a composed of intracellular and extracellular spaces; in monodomain model, it is assumed that the intracellular and extracellular domains are the same.[5]

At the tissue scale, cardiac tissue behaves like electrically coupled cells, and large-scale tissue simulations may involve millions of cells. Therefore, understanding cardiac behavior at the cell level and simplifying cell models are critical steps to improve computational tractability for the tissue models. Generally, biophysically detailed cell models include more than 30 variables, hundreds of equations and parameters; however, most simplified cell models only contains less than ten variables and a correspondingly reduced number of equations and parameters.[5]

Simplified models used for cardiac cell simulations are generally divided into three categories: *Reduced models*, *Generic model* and *Phenomenological models*.

Reduced models are direct reductions of the biophysically complex detailed cardiac models through using the steady-state value for the different variables, such as the fast gating variable that governs activation of current Na^+. Due to assuming that the gating variables instantaneously achieve the steady-state value that is related to a given voltage, the reduced models not only eliminate variables but also loose the significant properties. Therefore, the models are extremely sensitive to the time step, and a larger time step will result in unacceptably large errors. The main advantage of reduced models is to improve computational tractability and retain a similar structure as the detailed model; nevertheless, the approach may reduce or eliminate essential properties of real cells and tissue, which can lead to undesirable results.[5]

Generic model, also called generic excitable media models[5], describe a prototype of an excitable system like neuron or heart system. By modifying the parameters in the models, they can generate limited properties like the detailed models. The most representative *generic model* is the FitzHugh-Nagumo (the FHN) model[12] that is a 2-

variable reduction of the Hodgkin-Huxley model[18]. The FHN model and other generic models lack other critical realistic properties. For example they do not have relastic APD restitution curves. Therefore, it is limited to use and hard to show the qualitative behavior like the biophysically detailed models.[5]

Phenomenological models aim to reproduce main dynamical properties of cells and tissues without including extra biophysical details. For example, rather than containing ten or more ion channels, pumps and exchangers, phenomenological models focus on the summary of these properties such as fast inward, slow inward and slow outward currents that only depend on several variables and equations[10].

There are several pros of phenomenological models: First, The output of phenomenological models can fit not only the experimental data but also the biophysically detailed models. Moreover, these models only include the small number of variables, equations and parameters compared with the detailed models.[2]

1.2.1 Alternans in phenomenological models

Cardiac cellular electrophysiology models have been designed to represent cells from different regions (atria, ventricles, Purkinje) to different species (rabbits, zebrafish, and human). The number of phenomenological models has increased significantly in the past decade. However, a model for a specific combination of species and regions may still not be available. In some cases, only a small subset of models reproduce the particular properties like alternans for a given study[5]. As we mentioned before, T-wave alternans at fast pacing rates is a common phenomenon across many species and different regions of heart cells, but not all models have shown the existence of alternans. For example, alternans has been found in the canine ventricular model introduced by Fox *et al.* (2002)[13], but that has not been found in the earlier canine ventricular model created by Winslow model (1999)[36]. Among rabbit ventricular models, alternans exists in the model introduced by Mahajan *et al.* (2008)[22], but that has not been reported in

the earlier model proposed by Shannon *et al.* (2004)[28].

1.3   Metabifurcation analysis

Metabifurcation analysis was first introduced as a method to study a mean field model of the cortex (Liley's MFM).[14]. That model includes a bunch of nonlinear differential equations, several variables and a number of parameters, which is similar to the F-K model. Furthermore, the normal dynamical behavior of Liley's MFM is also periodic, which is similar to the F-K model. Based on these similarities, I have implemented the metabifurcation analysis in the F-K model, our goal is to disclose links between parameters and dynamical features like alternans and bistability.

In general, the metabifurcation analysis is implemented as follows:

• Search the parameter space of a model and find the meaningful combinations of parameters.

• Draw the bifurcation diagrams concerning one or two control parameters for all of the meaningful parameter sets.

• Partition the nonlinear structure of the selected parameter space in families according to different bifurcation responses.

• By comparing the distributions of parameters among the mentioned families, we can unveil the links between the parameters and the dynamical patterns; then, we can tell which parameters have the primary effect on the partitioning and cause the qualitative difference in dynamical behaviors.

1.4   Outline

The paper is divided into five main sections:

First, we analyze one of the human cardiac ventricular models, the F-K model (1998). We will show how $Ca^{[2+]}$, $Na^{[+]}$ and $Ka^{[+]}$ currents affect electrical events at a relatively

slow pacing frequency. As the pacing frequency increases, the physiological mechanisms causing alternans will be discussed.

Second, we introduce the theoretical and numerical tools employed in some details such as the time-step integration, particle swarm optimization(PSO), principal component analysis(PCA), etc. Furthermore, we will introduce some details about the bifurcation analysis of the F-K model.

Thirdly, there are three main steps in the implementation. The first is to search the parameter space with using a robust statistical method named the PSO procedure; as a result, we have obtained a large representative sample of parameter sets that can generate physiologically plausible behavior. The second step is to randomly choose a representative sample containing 270 thousand parameter sets. For each of these parameter sets, we draw the bifurcation plots showing the APD response to changes in the pacing frequency. The third step is to classify parameter sets into five "parent families", according to the number of period-doubling bifurcation points, and Fig. 1.2 indicates the three most common parent families. To understand the insightful behavior in the largest parent family(PF2) that only has one period-doubling bifurcation, we trace the other solution after the period-doubling bifurcation occurs. Consequently, we sort PF2 into four "distinct families" or "subfamilies". Fig. 1.3 shows the three most typical dynamical behaviors, and the last families includes the parameter sets with rare behaviors and convergence problems.

In the results, there are five major parts. First, after implementing the PSO process, we have obtained more than 1.5 million parameter sets, we talk about the distributions of parameters and relations among the parameters. Second, we show some illustrative bifurcation diagrams in parent families and subfamilies of PF2. Furthermore, we focus on the similarity and difference of the qualitative behaviors in four subfamilies belonging to PF2. Fourth, the parameter distributions in subfamilies are compared based Jensen-Shannon divergence. Finally, the relations between special points like period-doubling
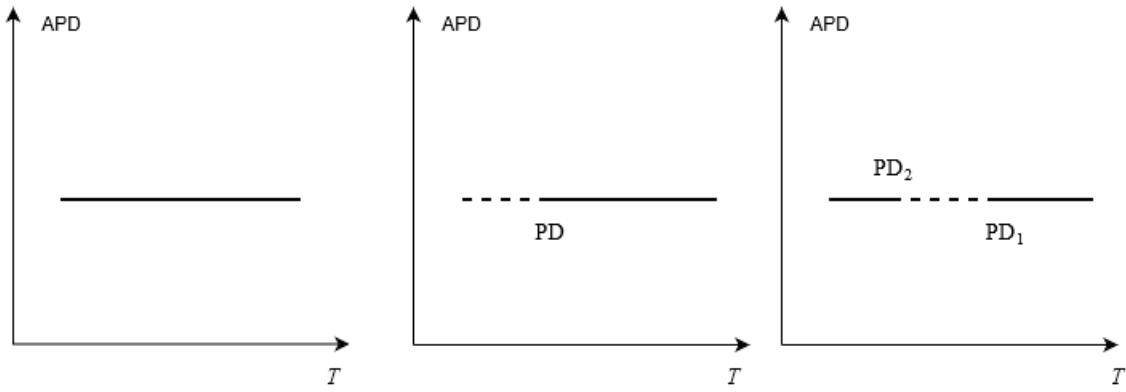
Figure 1.2: Family clasifications. Family classification is based on the number of period-doubling bifurcations(PD). Here, we show examples in three families: the first graph is PF1 witout period-doubling bifurcations; the second graph(PF2) has only one period-doubling bifurcation; the third one(PF3) has two period-doubling bifurcations
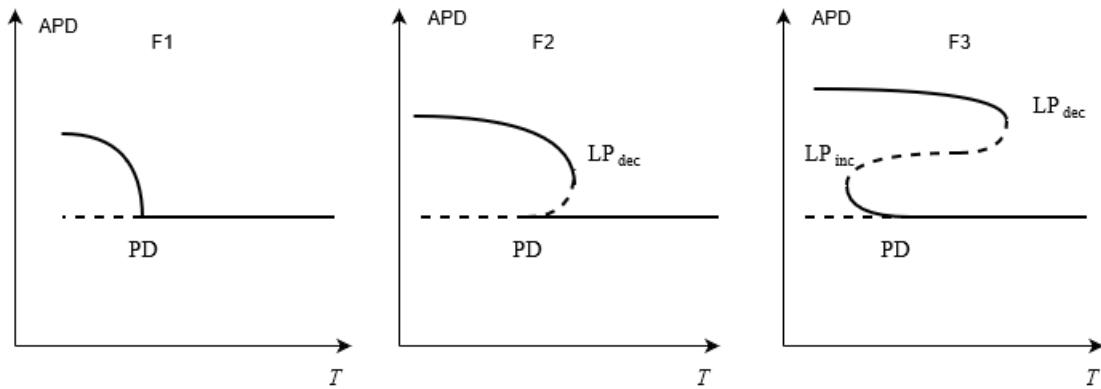
Figure 1.3: Subfamily clasifications in PF2. These three graphs show the classification in PF2 based on the behavior after switching branches at the period-doubling bifurcation. LP_{inc} is a fold bifurcation where the solution changes from stable to unstable; LP_{des} is a fold bifurcation where the solution changes from unstable to stable

bifurcations and parameters are discussed in each subfamily.

The last part is the discussion: First, to compare our approach and analysis with the former work that people have done, we talk about the contributions and the innovations of my research. Next, the results have been compared with some published results; some examples of the results have been discussed. Finally, the future work and its difficulties will be explained.

Chapter 2

The Fenton-Karma Model

2.1   Introduction of the F-K Model

Fenton and Karma (1998) have come up with the simplest phenomenological model of a cardiac membrane at both the ventricular cell level and the ventricular tissue level. The model has only three variables: u, v, and w. $u \equiv (V - V_c)/(V_{\text{fi}} - V_c)$ is a dimensionless membrane potential(Voltage) where V_c is a resting membrane potential, and V_{fi} is the potential of triggering a fast inward current; v is a fast gating variable; w is a slow gating variable.[10] Thirteen parameters are in Table. 2.1 and typical values for the parameters are used to draw the following graphs in Chapter 2.2 for analysis.

The three differential equations in the F-K model are shown in Eq.(2.1)$\sim$ Eq.(2.3):

$$\partial_t u = \bigtriangledown \cdot (D \bigtriangledown u) - J_{\text{fi}}(u; v) - J_{\text{si}}(u; w) - J_{\text{so}}(u) + J_{\text{stim}}(T) \qquad (2.1)$$

$$\partial_t v = \frac{1}{\tau_v^-(u)} \ominus (u_{\text{c}} - u)(1 - v) - \frac{1}{\tau_{\text{v}}^+} \ominus (u - u_{\text{c}})v \qquad (2.2)$$

$$\partial_t w = \frac{1}{\tau_{\text{w}}^-} \ominus (u_{\text{c}} - u)(1 - w) - \frac{1}{\tau_{\text{w}}^+} \ominus (u - u_{\text{c}})w \qquad (2.3)$$

First, voltage changing rate($\partial_t u$) depends on $\bigtriangledown \cdot (D \bigtriangledown u)$, J_{fi}, J_{si}, J_{so} and J_{stim} where J_{fi} represents a fast inward current (Na$^+$) depending on u and v, J_{si} shows a slow inward

Table 2.1: Physiological ranges and typical values for thirteen parameters of the F-K model.[3]

Parameter	Definition	Typical Values	Minimum	Maximum	Units
τ_{v1}^{-}	Reactivating time constant of the fast gating variable ($u < u_{v}$)	19.6	5	100	ms
τ_{v2}^{-}	Reactivating time constant of the fast gating variable ($u \geq u_{v}$)	1240	1	1500	ms
τ_{v}^{+}	Deactivating time constant of the fast gating variable	3.33	1	15	ms
τ_{w}^{-}	Reactivating time constant of the slow gating variable	41.0	10	150	ms
τ_{w}^{+}	Deactivating time constant of the slow gating variable	870.0	100	1000	ms
τ_{d}	Characteristic time of the fast inward current	0.25	0.05	0.3	ms
τ_{o}	Characteristic time of the slow outward current(reactivation)	12.5	5	25	ms
τ_{r}	Characteristic time of the slow outward current(deactivation)	33.33	15	250	ms
τ_{si}	Characteristic time of the slow inward current	29.0	15	55	ms
u_{crit}	Threshold of the fast inward current	0.13	0.1	0.25	
u_{c}^{si}	Threshold of the slow inward current	0.85	0.4	0.9	
u_{v}	splitting voltage	0.04	0.02	0.25	
k	Steepness of the slow inward current	10	8	20	

$*u_{c}^{\mathrm{si}} > u_{c} > u_{v}$

current (Ca^{2+}) affected by u and w, J_{so} indicates an outward current only relying on u, $\nabla \cdot (D \nabla u)$ represents spatial diffusion. Here, we analyze the F-K model without spatial extension; therefore, $\nabla \cdot (D \nabla u) \equiv 0$. Furthermore, we need to give an external periodic stimulus current J_{stim} [34] that represents the periodic excitation of the F-K model. The fast inward current, the slow inward current and the outward current are in Eq.(2.4)$\sim$ Eq.(2.6)

$$J_{fi}(u; v) = -\frac{1}{\tau_d} v \ominus (u - u_c)(1 - u)(u - u_c) \tag{2.4}$$

$$J_{si}(u; w) = -\frac{1}{2\tau_{si}} w(1 + \tanh[k(u - u_c^{si})]) \tag{2.5}$$

$$J_{so}(u) = \frac{1}{\tau_o} u \ominus (u_c - u) + \frac{1}{\tau_r} \ominus (u - u_c) \tag{2.6}$$

where τ_d is the characteristic time for the fast inward current, u_c is the threshold at which Na^+ channels are open, u_c^{si} is the threshold where Ca^{2+} channels are open, τ_{si} is a characteristic time for the slow inward current. τ_o and τ_r are the characteristic time of the slow outward current, $\ominus(x_1 - x_2)$ is the Heaviside step function, also named stepwise function, defined as:

$$\ominus(x_1 - x_2) = \begin{cases} 1 & x_1 \geq x_2 \\ 0 & x_1 < x_2 \end{cases} \tag{2.7}$$

Secondly, in Eq.(2.2), τ_v^+ is the time constant that governs the deactivation of the fast inward current, and $\tau_v^-(u)$ is also the time constant that controls the reactivation process of the same current separately over two voltage ranges ($u_v < u < u_c$ and $u < u_c$) by defining the function in Eq.(2.8):

$$t_v^-(u) = \ominus(u - u_v)\tau_{v1}^- + \ominus(u_v - u)\tau_{v2}^- \tag{2.8}$$

Third, in Eq.(2.3), τ_w^+ is the time constant that governs the deactivation of the slow outward current, and τ_w^- is the time constant controlling the reactivation of that current.
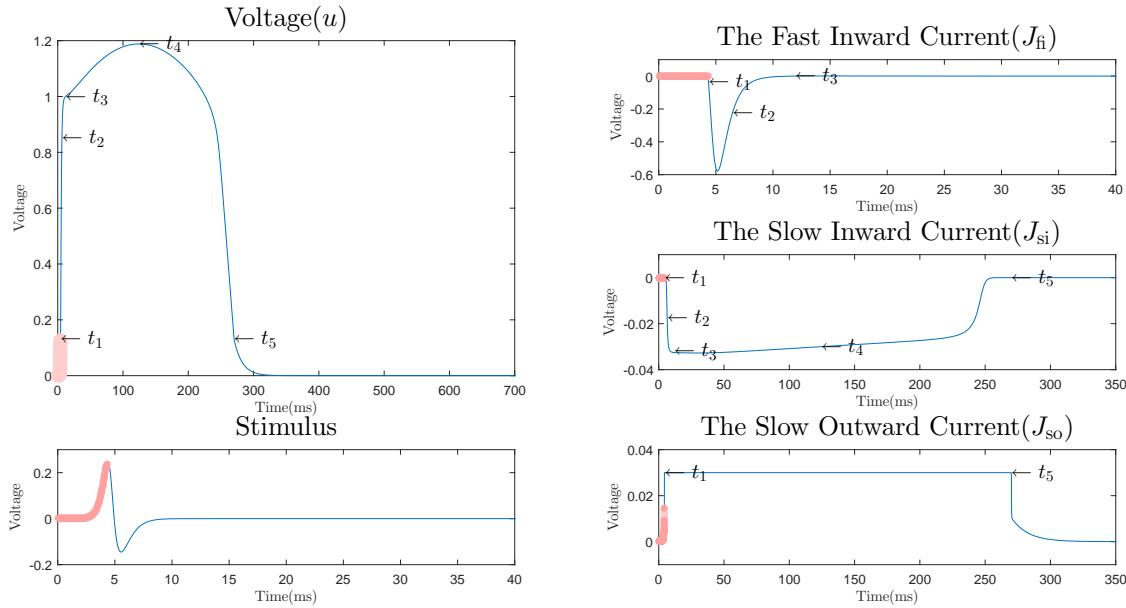
Figure 2.1: Membrane potential analysis for $0 < t \leq t_1$. The first graph shows how membrane potential changes with respect to time; the four small graphs show the four currents with respect to time. The pink line shows how the membrane potential changes corresponding to the four currents for $0 < t \leq t_1$. The values of parameters are from Table 2.1. To observe the changes clearly, the scales of the four currents are set differently

2.2   Analysis of the F-K Model

We will separately describe six phases of one periodic response. We trace time (t) from 0ms to 700ms that represents one period where $\triangle t$ is 0.05ms. In the following graphs from Fig. 2.1 to Fig. 2.6, t_1 and t_5 are the time at which the fast inward currents open and close, namely $u > u_{\text{crit}}$ and $u < u_{\text{crit}}$; t_2 is the time where slow inward currents open, $u > u_c^{\text{si}}$; t_3 is the time where $u > 1$ that is defined in Eq.(2.4); t_4 is the time where u passes the maximum value.

(1): $0 < t \leq t_1$

$$\partial_t u = -J_{\text{so}} + J_{\text{stim}} \approx J_{\text{stim}} \tag{2.9}$$
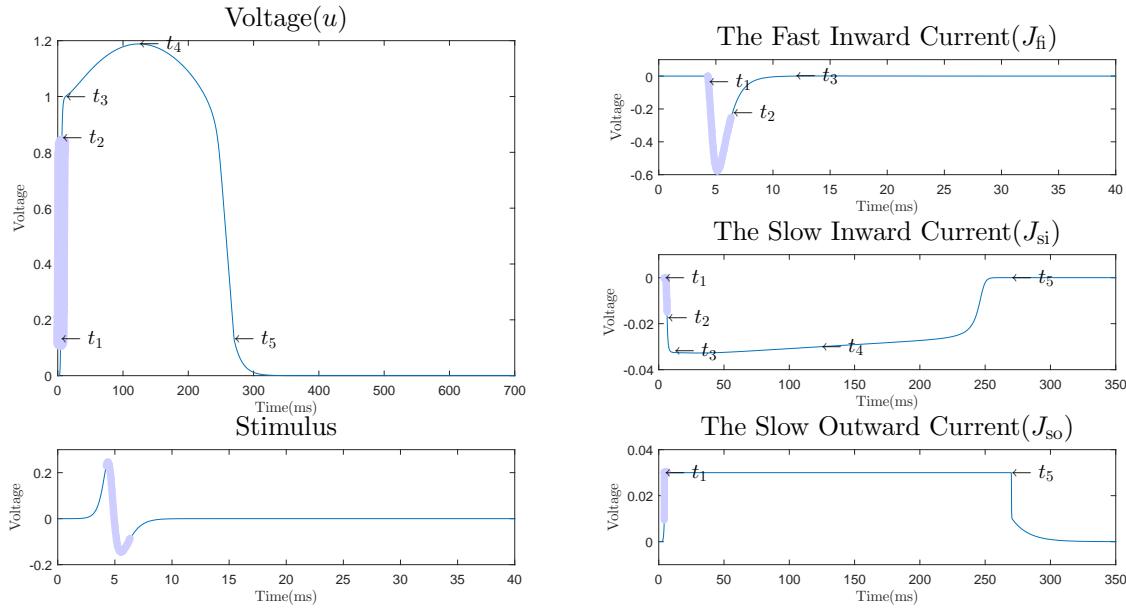
Figure 2.2: Membrane potential analysis for $t_1 < t \leq t_2$. The blue line shows how the membrane potential changes corresponding to the four currents J_{fi}, J_{si}, J_{so} and J_{stim} for $t_1 < t \leq t_2$.

According to equation Eq.(2.1)$\sim$ Eq.(2.3) and Fig. 2.1, when $0 < t \leq t_1$, $J_{\mathrm{fi}} = 0$, $J_{\mathrm{si}} = 0$ and $J_{\mathrm{so}} = -u/\tau_{\mathrm{o}} < 0.01$ is much smaller than the value of J_{stim}. Hence, the change of voltage is mainly dependent on J_{stim} shown in Eq. (2.9). Stimulus activates the voltage(u) to achieve the threshold of excitation (u_{crit}) to depolarize the membrane. Biochemically speaking, when $u < u_{\mathrm{crit}}$, the membrane potential is resting.

(2): $t_1 < t \leq t_2$

$$\partial_t u = -J_{\mathrm{fi}} - J_{\mathrm{si}} - J_{\mathrm{so}} + J_{\mathrm{stim}} \approx -J_{\mathrm{fi}} + J_{\mathrm{stim}} \tag{2.10}$$

In Fig. 2.2, when $t_1 < t \leq t_2$, the voltage(u) is greater than the threshold of excitation (u_{crit}) but smaller than $u_{\mathrm{c}}^{\mathrm{si}}$, the passage of Na$^+$ is open, and sodium ions enter the membrane. Simultaneously, the slow inward current is gradually activated; therefore, the passage of Ca^{2+} is slowly opening, and a few calcium ions pass through the membrane. During this period, $||J_{\mathrm{si}}|| < 0.02$ and $||J_{\mathrm{so}}|| = 0.03$ are much smaller than $||J_{\mathrm{fi}}||$ and $||J_{\mathrm{stim}}||$; therefore, the effect of the slow inward current and the slow outward current
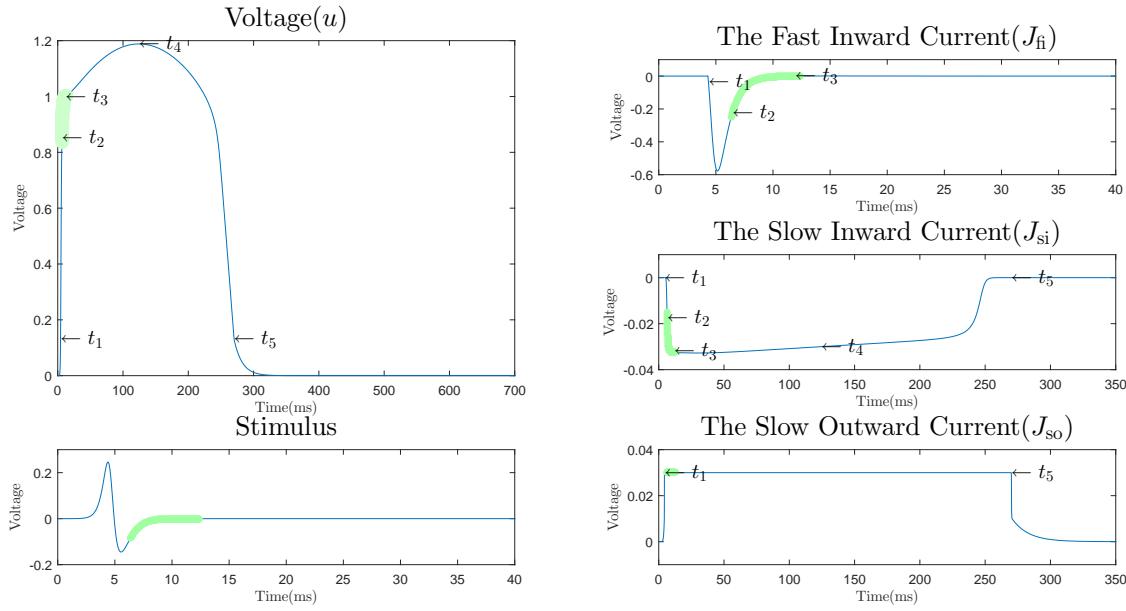
Figure 2.3: Membrane potential analysis for $t_2 < t \leq t_3$. The green line shows how the membrane potential changes corresponding to the four currents J_fi, J_si, J_so and J_stim for $t_2 < t \leq t_3$.

is negligible, and J_fi and J_stim have the key effect on the membrane potential shown in Eq.(2.10).

(3): $t_2 < t \leq t_3$

$$\partial_t u = -J_\text{fi} - J_\text{si} - J_\text{so} + J_\text{stim} \tag{2.11}$$

According to Fig. 2.3, when $t_2 < t \leq t_3$, the voltage(u) is greater than the threshold (u_c^si) of excitation of J_si but smaller than 1, the impact of the excitation current and the fast inward current is decreasing; in contrast, the effect of the slow inward current is increasing; furthermore, the slow outward current maintain the same impact. Biologically speaking, $t_2 < t \leq t_3$ is the transition time where the passages of Na$^+$ is gradually closing, and more and more channels of Ca^{2+} are open. Therefore, the slow outward and the slow inward currents slowly control the behavior of the membrane potential.
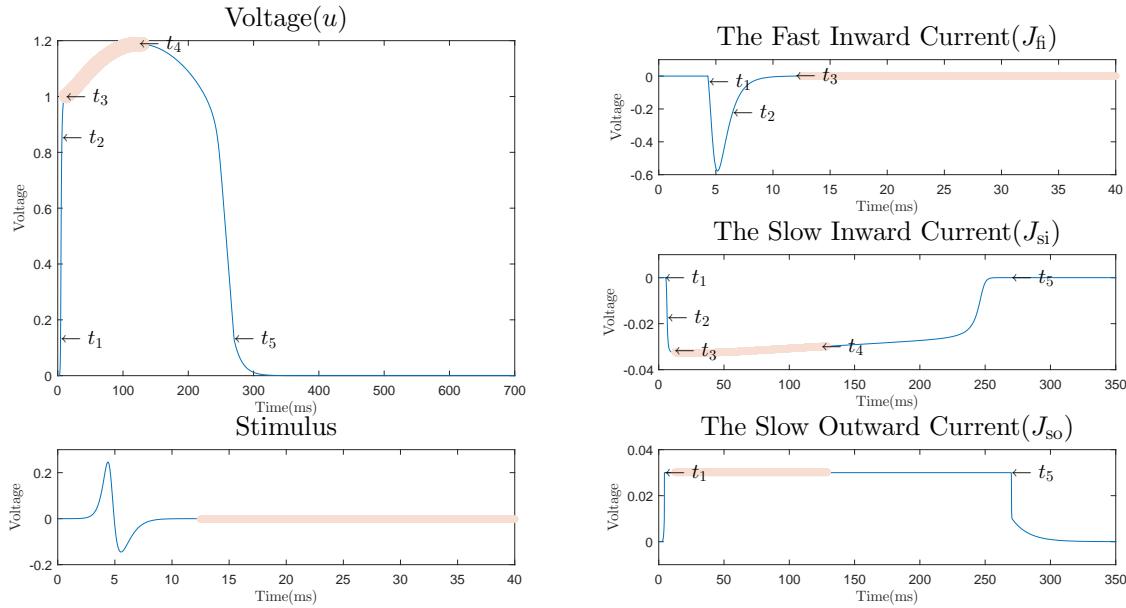
Figure 2.4: Membrane potential analysis for $t_3 < t \leq t_4$. The brown line shows how the membrane potential changes corresponding to the four currents J_{fi}, J_{si}, J_{so} and J_{stim} for $t_3 < t \leq t_4$.

(4) $t_3 < t \leq t_4$

$$\partial_t u = -J_{\text{si}} - J_{\text{so}} \tag{2.12}$$

When $t_3 < t \leq t_4$, $1 < u < u_{\max}$ and the channels of sodium ions are completely closed, and u only depends on the slow inward current and the slow outward current shown in Eq.(2.12). In Fig. 2.4, $||J_{\text{si}}||$ is decreasing; in contrast, $||J_{\text{so}}|| = 0.03$ is constant. When $||J_{\text{si}}|| > ||J_{\text{so}}||$, the voltage increases from 1 to $u_{\max} = 1.18$; when $||J_{\text{si}}|| = ||J_{\text{so}}||$, $\partial_t u = 0$, the voltage reaches the maximum point, and the membrane finishes the depolarization.

(5) $t_4 < t \leq t_5$

$$\partial_t u = -J_{\text{si}} - J_{\text{so}} \tag{2.13}$$

When $t_4 < t \leq t_5$, u is decreasing from $u_{\max}$ to the threshold u_{crit} where $||J_{\text{si}}|| < ||J_{\text{so}}||$. At the beginning, the channel of Ca^{2+} closes slowly; then, the closing speed increases so
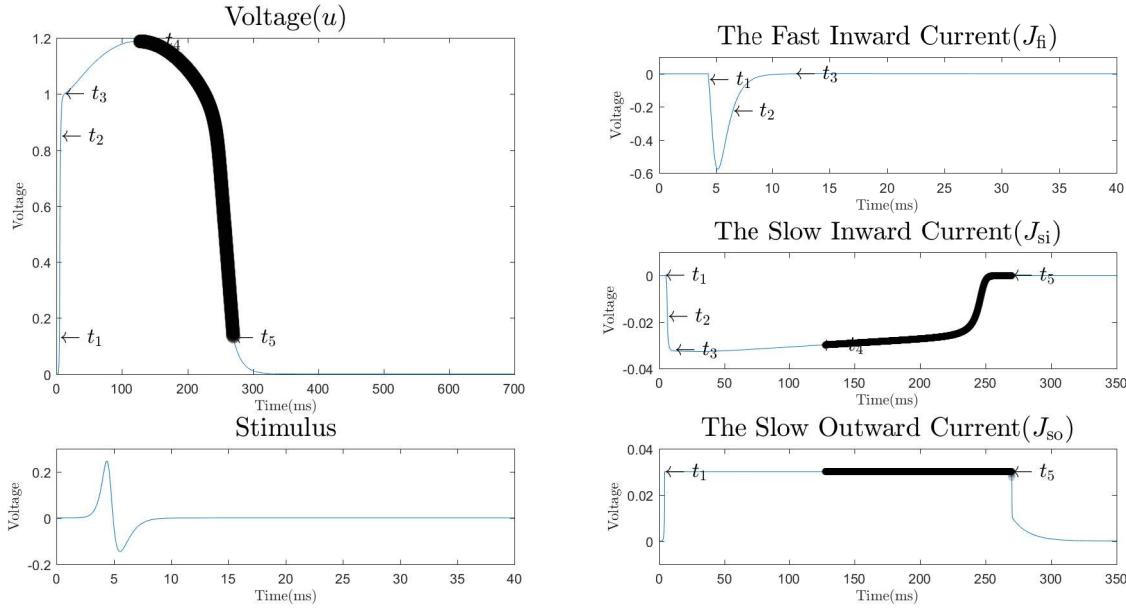
Figure 2.5: Membrane potential analysis for $t_4 < t \leq t_5$. The black line shows how the membrane potential changes corresponding to the four currents J_{fi}, J_{si}, J_{so} and J_{stim} for $t_4 < t \leq t_5$.

the impact of the slow inward current is reducing during this phase. However, the effect of the slow outward current maintains the same. According to Eq.(2.13) and Fig. 2.5, we can see that the change of voltage(u) still depends on J_{si} and J_{so} but gradually depends on J_{so} only.

(6)$t_5 < t$

$$\partial_t u = -J_{\text{so}} \tag{2.14}$$

When u is close to u_{crit}, the channel of Ca^{2+} has completely closed, and the only open channel is K^+. In 2.14 and Fig. 2.6, u only depends on J_{so}. As $t_5 < t$, u is smaller than u_{crit} again, the speed of K^+ leaving the membrane significantly decreases, and u gradually restores to the resting membrane potential.

During those aforementioned six stages, (1) $\sim$ (4) are the processes of depolarization; in comparison, (5) $\sim$ (6) implement the repolarization. We have analyzed how the membrane potential u changes corresponding to the two gating variables v and w in one
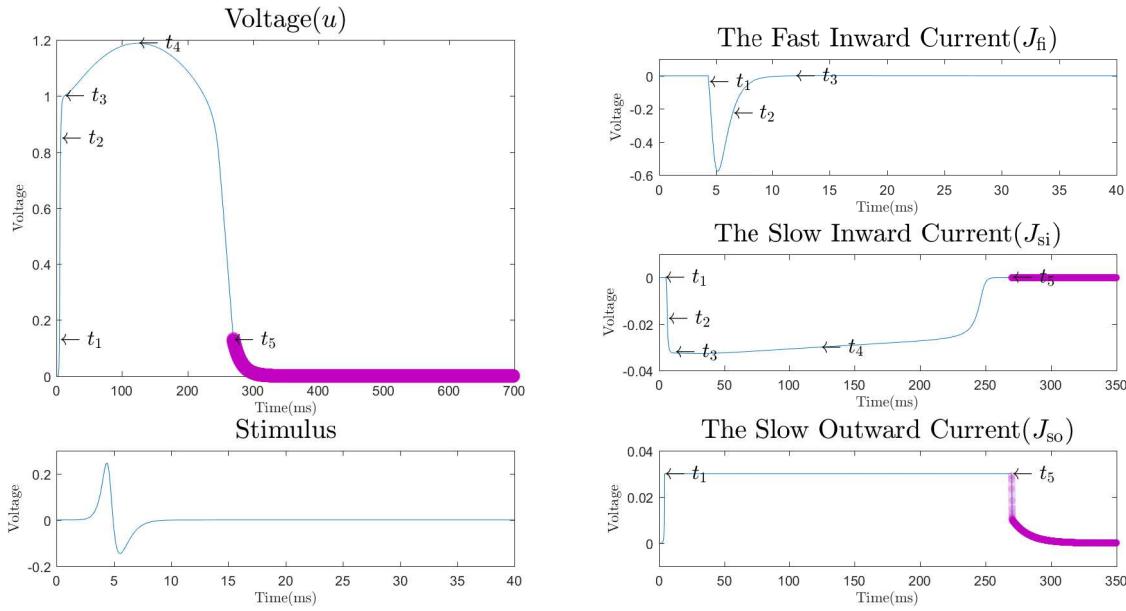
Figure 2.6: Membrane potential analysis for $t_5 < t$. The purple line shows how the membrane potential changes corresponding to the four currents J_{fi}, J_{si}, J_{so} and J_{stim} for $t_5 < t$.

period, and the graph is in Fig. 2.7.

The fast gating variable and the slow gating variable control the fast inward current and the slow inward current separately. Therefore, if two gating variables do not have enough time to rest; as a consequence, the next response will be abnormal. We will talk about this phenomenon in the following section.

2.3 Behaviors of the F-K model with the increasing pacing frequency

As the pacing frequency increases, there is not enough time for both gating variables to recover completely. Consequently, alternans will appear, which corresponds to a period-doubling bifurcation point in bifurcation analysis.

In general, a bifurcation occurs when a small smooth change made to the control parameter value of a system causes a sudden 'qualitative' or topological behavior change
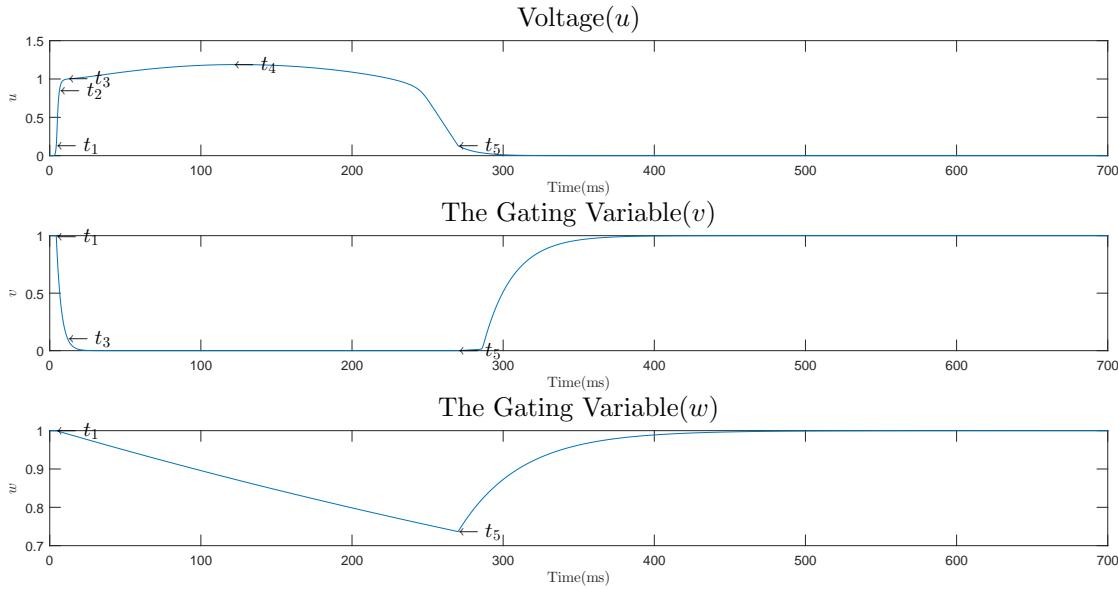
Figure 2.7: The curves of three variables in one period. The first graph is the voltage(u), the second one is the fast gating variable(v), and the last one is the slow gating variable(w) during one period (700 ms)

in its dynamical behavior[23]. In the F-K model, when the forcing period T as a control parameter decreases, the behavior of the model will change qualitatively to alternating behavior when a period-doubling bifurcation appears.

In Chapter 1.1, we have mentioned cycle length (CL=APD+DI), and we can also call the CL as forcing period T. In one CL, the longer APD needs more time to recover. If the DI is longer than the recovering time, the APD of the next CL will not be affected; in contrast, if the DI is not long enough to cover the recovering time, the APD of the next CL will be affected and becomes shorter. Fig. 2.8 shows both cases.

As T decreases, the APD does not change because the DI is longer than the recovering time; therefore, the behavior of the electric system of a ventricular cell will not change qualitatively.

If the pacing time T still decreases, the DI is not long enough time to cover the recovering time. The APD of the next cycle length(CL) will be affected and become
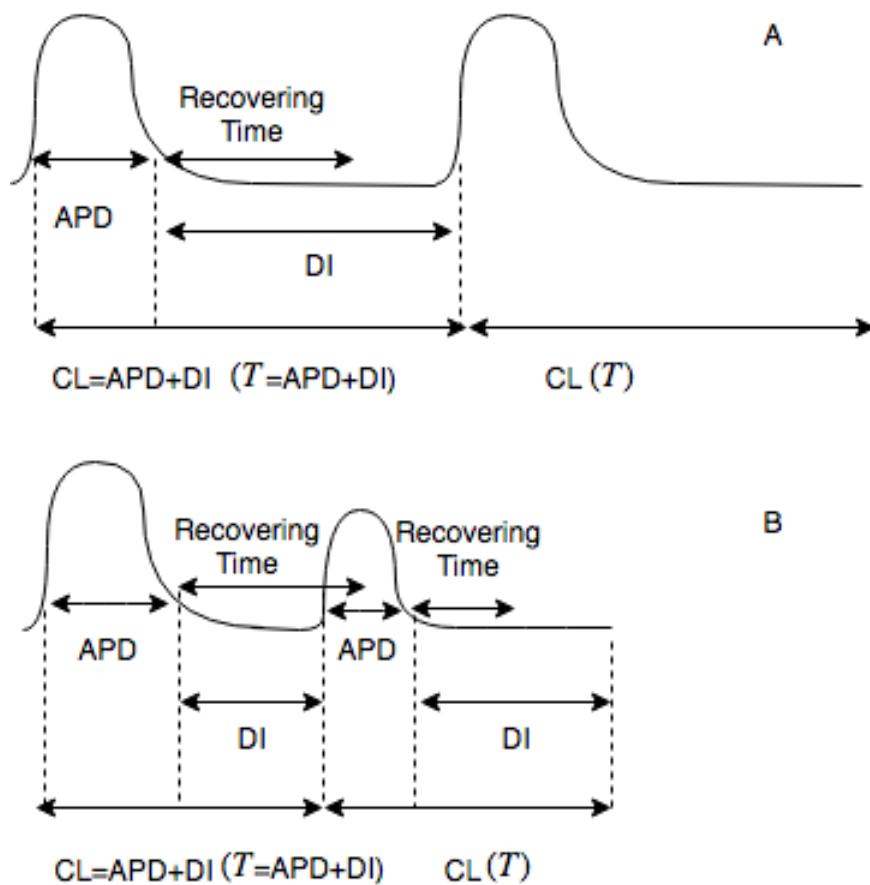
Figure 2.8: Behaviors of the longer cycle length(CL) and the shorter CL. A illustrates the behavior that DI is long enough to cover the recovering time; B shows the behavior that the DI is not long enough to cover the rescovering time

shorter. As we mentioned the shorter APD requests less time to recover; namely, the second APD needs less time to restore. Therefore, the DI of the second CL is long enough to give the ventricular cell enough time to repolarize. Consequently, the the third cycle length will be like the first cycle length, and the fourth CL will be like the second one. This physiological behavior is called alternans; we can observe the onset of the alternans after the first period-doubling bifurcation appears in general.

As the T continuously decreases, the DI in the second cycle length(CL) is not long enough to cover the recovering time to generate the normal APD in the third CL. Therefore, the third ADP decreases and the time needed for the repolarization also reduces, so we will see the behavior of the third CL gradually approach that of the second CL. In a nutshell, all CLs will behave as the same again. It means the alternans disappears when we decrease T at some specific value. Correspondingly, we will see the second period-doubling bifurcation point in the F-K model.

We have explained the dynamical behavior as we decrease the forcing period T by illustrating one example. If we choose another parameter set, the behavior will possibly be different. For example, we may not see the absence of alternans. In some parameter sets, the behavior that alternans appears and disappears may repeat as T decreases as long as the forcing time is long enough to ensure $T > APD$. Otherwise, there will be two stimuli corresponding to one CL because the second stimulus occurs during the same APD restitution curve, and it diminishes suddenly and cannot generate the second APD restitution curve. We call this forcing period as blocking time. Different parameter sets will make the F-K model behavior differently as T decreases. We will see more types of behaviors in Chapter 5.

Chapter 3

Numerical methods

3.1 Time-step Integration

In the last chapter, we have introduced the F-K model, we can write the nonlinear differential equations of the F-K model as Eq.(3.1)

$$\dot{X} = F(X) \tag{3.1}$$

where $F(X)$ are the differential equations from Eq.(2.1)$\sim$ Eq.(2.3), $X = (u, v, w)$.

When we do the bifurcation analysis as the control parameter T varies, the fixed point at each T is obtained by solving the linearized ODEs with Newton's method. To solve the linearized ODEs, we need to compute the matrix of derivative of the map $\phi(t)$. To find that matrix, we need to solve the linearized differential equations of the F-K model in Eq.(3.2)

$$\dot{A} = D_X F(\phi(t)) A \tag{3.2}$$

where $A = D_X \phi(t)$, and $\phi(t)$ is the solution. $D_X F(\phi(t))$ is a 3×3 Jacobian matrix.

3.1.1 Time-stepping methods

In numerical analysis, Runge-Kutta methods are a family of implicit and explicit iterative methods used in temporal discretization for approximate solutions of ordinary differential equations [6]. The forward Euler method is the most basic explicit method for numerical integration of ordinary differential equations and the simplest Runge-Kutta method shown in Eq.(3.3)

$$X^{i+1} = X^i + F(X^i) \cdot h \tag{3.3}$$

where $X = (u, v, w)$, $F(X)$ is the vector of $(\dot{u}, \dot{v}, \dot{w})$, and $h = dt$ in the F-K model.

The trapezoidal rule is an implicit second-order method, which can be considered as both a Runge-Kutta method and a linear multistep method. We discretize Eq.(3.1) with the trapezoidal rule, we will get Eq.(3.4).

$$X^{i+1} = X^i + \frac{1}{2}(F(X^i) + F(X^{i+1})) \cdot h \tag{3.4}$$

In the bifurcation analysis of the F-K model, we also use the trapezoidal rule to discretize Eq.(3.2) and get Eq.(3.5).

$$A^{i+1} = A^i + \frac{1}{2}(D_{X^i}F(X^i)A^i + D_{X^{i+1}}F(X^{i+1})A^{i+1}) \cdot h \tag{3.5}$$

There are three reasons that we choose the trapezoidal rule rather than other Runge-Kutta methods:

• Computational efficiency: as we know, the higher the order of Runge-Kutta methods we use, the faster the error is reduced as the time step decreases. However, we will search millions of parameter sets of the F-K model, and we will integrate thousands of time steps for each parameter set. To improve computational efficiency and make the particle swarm optimization(PSO) executable efficiently, we choose the second order accuracy Runge-Kutta method.

• Accuracy: the accuracy of the Euler method improves linearly when the step size decreases linearly, whereas the trapezoidal method enhances the accuracy quadratically. Because we will do bifurcation analysis on the F-K model, we need a relatively accurate prediction in each time step.

• Stability: We have shown that the F-K model includes several stepwise functions. To make the system differentiable, we convert them to the hyperbolic tangent functions with a large stiffness parameter k^{step}. Due to this, we need a stable time-stepping method. The trapezoidal rule is a relatively stable multi-time-step method [32].

3.1.2   Newton's method

Newton's method, also named the Newton-Raphson method, is a method for finding successively better approximations to the roots of a function.

In the F-K model, we use Newton's method to solve the trapezoidal rule to find a more accurate solution. In each time step, we would like to solve Eq.(3.6). Because the trapezoidal method is an implicit method, we use the forward Euler method to obtain the adequately good initial guess of X_{n+1}^0.

$$G(X_{n+1}^i, X_n, t_n, t_{n+1}) = X_{n+1}^i - \frac{1}{2}(F(X_n, t_n) + F(X_{n+1}^i, t_{n+1})) \cdot dt - X_n = 0 \qquad (3.6)$$

where $X_n = (u_n, v_n, w_n)$, $dt = t_{n+1} - t_n$ and $F(X, t) = (\dot{u}, \dot{v}, \dot{w})$.

To solve the Eq.(3.6), we need compute Z in the linear equations $AZ = B$ shown as Eq.(3.7).

$$\nabla_{X_{n+1}^i} G(X_{n+1}^i, X_n, t_n, t_{n+1})(X_{n+1}^{i+1} - X_{n+1}^i) = -G(X_{n+1}^i, X_n, t_n, t_{n+1}) \qquad (3.7)$$

where $A = \nabla_{X_{n+1}^i} G(X_{n+1}^i, X_n, t_n, t_{n+1})$, $Z = (X_{n+1}^{i+1} - X_{n+1}^i)$, and $B = -G(X_{n+1}^i, X_n, t_n, t_{n+1})$.

$$X_{n+1}^{i+1} = X_{n+1}^i + \triangle X_{n+1}^i \tag{3.8}$$

where $\triangle X_{n+1}^i = X_{n+1}^{i+1} - X_{n+1}^i$.

After solving Eq.(3.7) in one iteration, we can get a better approximation of X_{n+1} in Eq.(3.8) if Newton's method converges. Then, we can move to the next iteration until the error is smaller than the error we set.

$$[I_{3\times3} - \frac{1}{2}dt D_{X^{i+1}}F(X^{i+1})]A^{i+1} = [I_{3\times3} + \frac{1}{2}dt D_{X^i}F(X^i)]A^i \tag{3.9}$$

After getting X_{n+1} by solving Eq.(3.4) with Newton's iteration, Eq.(3.9) shows how to solve Eq.(3.5) to get A^{i+1}.

3.2 Particle Swarm Optimization

Particle swarm optimization (PSO) is a swarm intelligence technique for optimization initially developed by Kennedy and Eberhart(1995) [20]. PSO searches a solution space for optimizing a problem by iteratively updating candidate solutions according to the given function that measures the behavior of each candidate solution. The position of a candidate solution is affected not only by its local best position but are also guided toward the global best location in the searching space. Eventually, all candidate solutions may or may not move toward the global best solution depending on the perturbation.

The PSO system is consisting of two equations: First is the velocity updated equation given by Eq.(3.10), and the position is updated with Eq.(3.11).

$$V_i^{t+1} = V_i^t + R_1 d_t(\text{LP}_i - P_i^t) + R_2 d_t(\text{GP}^t - P_i^t) \tag{3.10}$$

$$P_i^{t+1} = P_i^t + V_i^{t+1} \tag{3.11}$$

where the index of a particle is represented by i. $V_i^t = (v_i^t(1), v_i^t(2), ...v_i^t(m))$ is the velocity of particle i at t where t is an integer and represents each PSO step; m is the number of dimensions. $P_i^t = (p_i^t(1), p_i^t(2), ...p_i^t(m))$ is the location of particle i at time t, $GP^t = (gb^t(1), gb^t(2), ...gb^t(m))$ is the global best position of all particles at time t, and $LP_i^t = (lp_i^t(1), lp_i^t(2), ...lp_i^t(m))$ is the local best position of each particle until time t. $R_1 = (r_1^t(1), r_1^t(2), ...r_1^t(m))$ and $R_2 = (r_2^t(1), r_2^t(2), ...r_2^t(m))$ are the perturbation vectors and each element of the vectors is selected from a (0,1) uniform distribution.   In the F-K model, a particle represents a parameter set where each dimension of the particle indicates each parameter.

Shi and Eberhart(1998)[30] came up with the concept of an inertia weight ω by introducing a constant parameter in the PSO procedure, which significantly affects the convergence and exploration ability. Therefore Eq.(3.10) turns to Eq.(3.12)

$$V_i^{t+1} = \omega V_i^t + R_1 d_t(LP_i^t - P_i^t) + R_2 d_t(GP^t - P_i^t) \tag{3.12}$$

They stated that a large inertia weight facilitates a global search while a small inertia weight facilitates a local search[30].   When ω equals 0, the previous velocity will not influence the current velocity, and we can rewrite Eq.(3.11) and (3.12) to Eq.(3.13).

$$P_i^{t+1} = P_i^t + R_1 d_t(LP_i^t - P_i^t) + R_2 d_t(GP^t - P_i^t) \tag{3.13}$$

In Eq.(3.13), $\omega = 0$ that means there is not inertia anymore, so the current position of a particle only depends on the previous position, the local best location, the global best position and the step size; therefore, the local searching ability significantly improves. For different purposes, parameter sets are scored by different criteria; here, the score, given in Eq.(4.18) in Chapter 4, is based on the APD that each parameter set can generate. Eq.(3.13) is not a simple and convex function with global optimum, and the global best

position is the best position among the local best positions in each PSO step, and there can be many global best positions that have the same score.

3.3 Principal Component Analysis

Karl Pearson(1901)[25]invented principal component analysis (PCA) which is a statistical procedure with using an orthogonal transformation to convert a set of observed data of correlated variables into a set of linearly uncorrelated variables.

It is defined that the first principal component has the largest possible variance and the following components have the smaller variance compared with the preceding components. Since each component is orthogonal to the others, the resulting variables form an uncorrelated orthogonal basis set.

PCA can be implemented by eigenvalue decomposition of a data covariance matrix after normalizing the data matrix for each variable. The results of PCA procedure will be expressed as component scores or factor scores and the variable values corresponding to the scores[29].

The procedure of PCA with the covariance method is explained as follows:

Let P be a matrix with m dimensions as colomns and n observations as rows. In the F-K model, m is the number of parameters, and n is the number of parameter sets. First, standardize the components of matrix, each standardized component is:

$$\widehat{p_j^i} = \frac{(p_j^i - \overline{p_j})}{\sigma(p_j)} \tag{3.14}$$

where i is the index of the observation, j is the index of the dimension, $\sigma(p_j)$ is the standard deviation and $\overline{p_j} = \dfrac{1}{n}\sum_{i=1}^{n} p_j^i$.

Second, we compute the covariance matrix C that is a $m \times m$ matrix where each element represents the covariance between two features. The covariance between two features is computed as follows:

$$c_{jh} = \sum_{i=1}^{n} \frac{(\widehat{p}_j^i - \overline{p_j})(\widehat{p}_h^i - \overline{p_h})}{n} \tag{3.15}$$

and the covariance matrix C is:

$$C = (c_{jh})_{m \times m} = \begin{bmatrix} c_{11} & c_{12} & ... & c_{1m} \\ c_{21} & c_{22} & ... & c_{2m} \\ . & . & . & . \\ . & . & . & . \\ . & . & . & . \\ c_{m1} & c_{m2} & ... & c_{mm} \end{bmatrix}$$

Next, we implement the eigen-decomposition on the covariance matrix to get eigen-values and eigenvectors. The magnitude of the eigenvalues measures the amount of information that different eigenvectors can present. According to the percentage of each absolute eigenvalue occupying among all the absolute eigenvalues, we can tell the portion of information that each eigenvector can explain.

3.4   Bifurcation Analysis of the F-K model

In the F-K model or other phenomenological models, the qualitative behaviors changing in a ventricular cell are related to bifurcation points in bifurcation analysis. The following steps show the way that we design our dynamical system and do the bifurcation analysis.

3.4.1   Poincaré Map

Our system is designed as a Poincaré map that can be interpreted as a discrete dynamical system. In the F-K model, we can consider the time-step integration in one period as a map $\phi(X, t)$ where X is a vector of variables (u, v, w) and t is the evolution time. The map $\phi(X, t)$ satisfies Eq.(3.16):

$$\frac{\partial}{\partial t}\phi(X,t) = \dot{X} = \begin{bmatrix} \partial_t u \\ \partial_t v \\ \partial_t w \end{bmatrix} = \begin{bmatrix} -J_{\mathrm{fi}}(u;v) - J_{\mathrm{si}}(u;w) - J_{\mathrm{so}}(u) + J_{\mathrm{stim}}(T) \\ \dfrac{1}{\tau_v^-(u)} \ominus (u_{\mathrm{c}} - u)(1-v) - \dfrac{1}{\tau_v^+} \ominus (u - u_{\mathrm{c}})v \\ \dfrac{1}{\tau_w^-} \ominus (u_{\mathrm{c}} - u)(1-w) - \dfrac{1}{\tau_w^+} \ominus (u - u_{\mathrm{c}})w \end{bmatrix} \quad (3.16)$$

In my research, we numerically solve Eq.(3.16) in the F-K model by the mentioned time-step integration in one period T and get Eq.(3.17):

$$\phi(X,T) : X^n \to X^{n+1} \tag{3.17}$$

$$G(X,T) = \phi(X,T) - X = 0 \tag{3.18}$$

To attain the fixed point X, we implement Newton's method to solve Eq.(3.18) to obtain a better approximation of the fixed point in each iteration.

3.4.2   Phase condition

In the bifurcation analysis, we would like to analyze how the control parameter T affects the map, so we not only need to obtain a better approximation of the fixed X but also need to find a better approximation of T that is consider as a variable as follows. In the map of the F-K model, Eq.(3.19) has three ordinary differential equations but four variables.

$$G(X,T) = \phi(X,T) - X = 0 \tag{3.19}$$

Therefore, we need to introduce a phase condition to a unique solution. There are different ways to define the last equation to find the solution $Z = (X,T)$. In AUTO, if we give Eq.(3.19)$\mathbb{R}^4 \to \mathbb{R}^3$, AUTO will create the last equation Eq.(3.20): $\mathbb{R}^4 \to \mathbb{R}^1$.
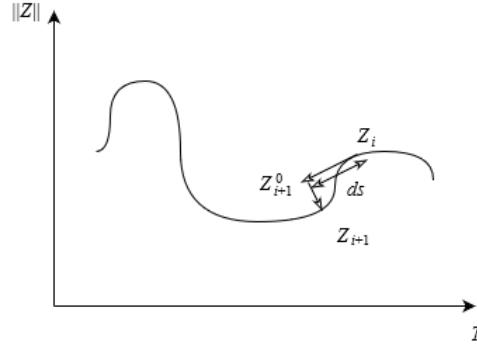
Figure 3.1: Solution curve of the F-K model. The x-axis is the periodic stimulus time T, the y-axis is the L_2 norm of the vector Z. Z_i is the solution we know; Z_{i+1}^0 is a proposed solution; Z_{i+1} is a new solution; ds is the pseudo arclength.

In Fig. 3.1, $\psi(X,T)$ is chosen as a vector (Z_i, Z_{i+1}^0), where Z_{i+1}^0 is a proposed point, is perpendicular to (Z_{i+1}^0, Z_{i+1}) where Z_{i+1} is a new point. In AUTO, $\psi(X,T)$ is defined such that the distance between Z_{i+1}^0 and Z_{i+1} is minimal.

$$\psi(X,T) = 0 \tag{3.20}$$

Now, we have four equations and four variables so we can use Newton's method to solve Eq.(3.19) and Eq.(3.20) to get a better approximation of Z. A sketch of a solution curve of Z is in Fig. 3.1

In Fig. 3.1, ds is defined as

$$ds = \parallel Z_{i+1}^0 - Z_i \parallel \tag{3.21}$$

In AUTO, the pseudo-arclength is adjustable, if Newton's iteration converges very fast, then ds will increase until it reaches the maximum ds; in contrast, if Newton's iteration cannot converge, ds will decreases until reaching the minimum ds.
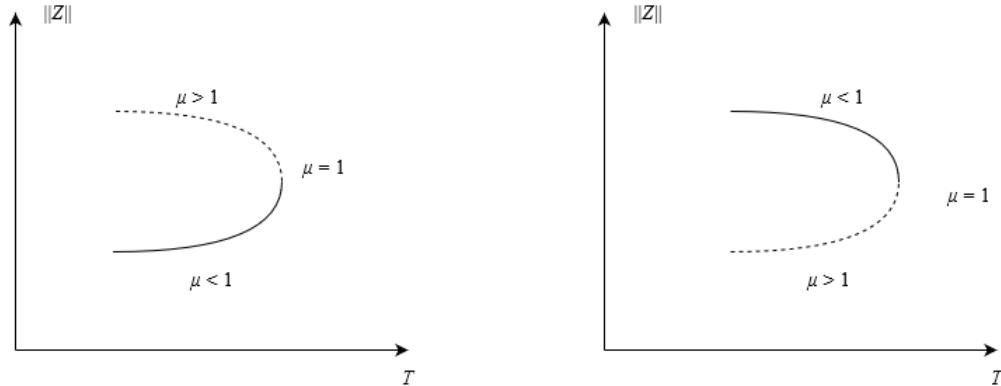
Figure 3.2: Fold bifurcations in the F-K model. If we trace the solution from the upper branch to the lower branch, the first graph shows a solution that changes from unstable to stable when multiplier μ passes one, and the second graph indicates a solution that changes from stable to unstable when the multiplier changes from $\mu < 1$ to $\mu > 1$.

3.4.3 Fold bifurcation

In bifurcation theory, a local bifurcation where two equilibrium points of a dynamical system collide with each other is named saddle-node bifurcation point. In discrete dynamical systems, the same bifurcation is often instead named a fold bifurcation.

In the mentioned discrete dynamical system, we have defined our map in Eq.(3.22):

$$\phi(X, T) : X^n \to X^{n+1} \tag{3.22}$$

To solve the fixed point X, we need to solve Eq.(3.23).

$$G(X, T) = \phi(X, T) - X = 0 \tag{3.23}$$

where X is the fixed point. When one eigenvalue of the Jacobian matrix $D\phi(X, T)$ passes 1, we can tell the equilibrium point has a fold bifurcation. Fig. 3.2 illustrates the fold bifurcation.
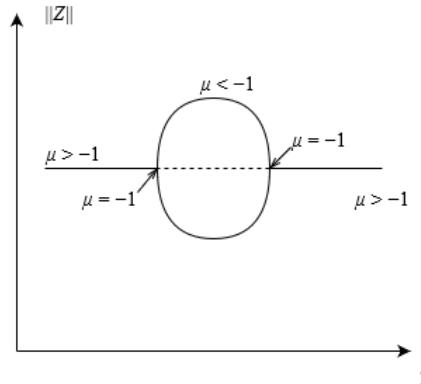
Figure 3.3: Period-doubling bifurcations in the F-K model. From left side to right side, the first $\mu = -1$ is a period-doubling bifurcation that indicates a stable alternating solution appears, and the second $\mu = -1$ is another period-doubling bifurcation in which a stable alternating solution disappears.

3.4.4 Period-doubling bifurcation

In discrete dynamical systems, period-doubling bifurcation is a bifurcation where a slight change in a parameter value will result in the original periodic system switching to a new behavior with twice the period of the original system.

When one eigenvalue of the Jacobian matrix $D\phi(X, T)$ passes -1, we can tell the equilibrium point has a period-doubling bifurcation. Fig. 3.3 shows the stable alternating solution appearing and disappearing concerning the value of multiplier μ.

3.5 OpenMP and Open MPI

OpenMP (Open Multi-Processing) is an application programming interface (API) that supports multiple platforms executes tasks by using shared memory in C, C++, and Fortran[31]. OpenMP is implemented by using multi-threads that share the same memory space to execute a task where a master thread (a series of instructions executed sequentially) forks a number of slave threads, and the master thread distributes parallel
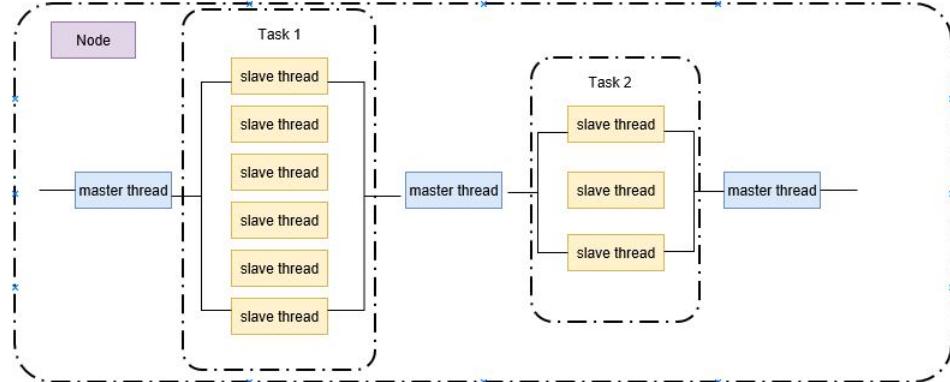
Figure 3.4: Slave node including a master thread and multiple slave threads implements a parallel task with OpenMP. Task 1 and Task 2 are two different parallel tasks.

sub-tasks to the slave threads; then, the slave threads can run the parts of the whole task concurrently. The process is shown in Fig.3.4.

Compared with OpenMP, Open MPI is an interface among different CPUs(CPUs) without sharing memory space. One CPU that is considered as the master node sending distributes tasks to other CPUs that are slave CPUs. When the slave processors finish their tasks, they will send the results back to the master node, and the master node will execute the subsequent instructions.

In general, the application programming that is built with the hybrid model of both OpenMP and OpenMPI where OpenMP is used for parallelism within a (multi-threads) node while Open MPI is for parallelism among all CPUs.

The reason that we choose OpenMP and Open MPI is to speed up the PSO searching process. Here is an example that we set 200 particles and update 5 PSO steps. Fig. 3.6 and Fig.3.7 show CPU time VS different numbers of CPUs and threads.
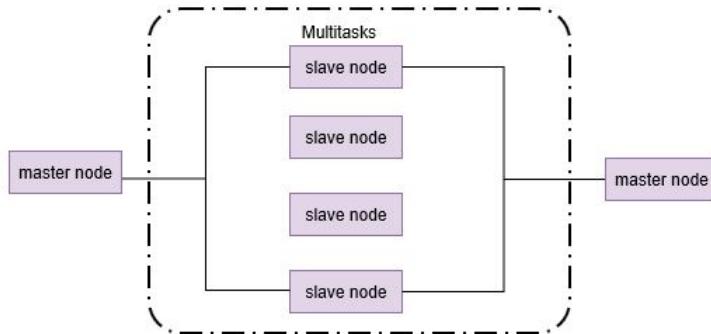
Figure 3.5: Master node distributes multitasks to slave CPUs and obtains the results from slave CPUs with Open MPI. Multitasks can be totally different.
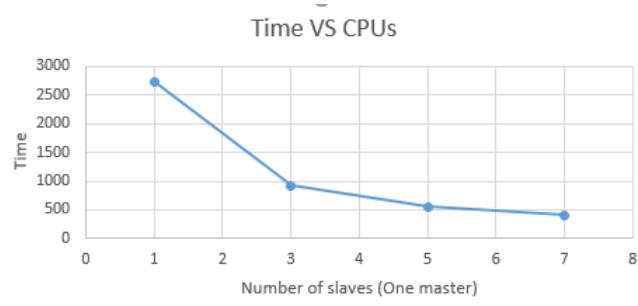
Figure 3.6: CPU Time VS the number of CPUs One CPU is set as master, the number of slaves increases from 1 to 7, and each slave CPU only has one thread
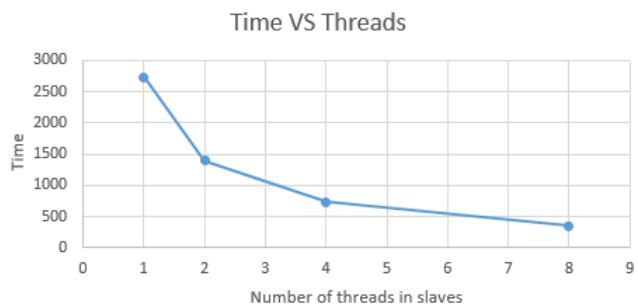
Figure 3.7: CPU Time VS the number of threads. One CPU is set as master, one CPU is set as slave, and the number of threads in the slave CPU increases from 1 to 8

3.6   Language and Software

Fortran developed by IBM is an imperative programming language that is especially used for scientific computing and numerical computation. The reason of using Fortran or C++ rather than Matlab or other high level languages is that Fortran or C++ is a low level language that is faster than the high level languages in terms of computation; furthermore, we set multiple tasks in PSO implementation to search parameter space in order to speed up the searching ability; therefore we have to use OpenMP and Open MPI that other advanced languages cannot execute. The other reason of choosing Fortran rather than other low level languages for my research is that AUTO files are written in Fortran.

AUTO is a software that is designed for continuation and bifurcation problems in ordinary differential equations. AUTO-07p is the latest version[7]. When we do the bifurcation analysis, the time-step integration will be a subroutine that must be Fortran file to be compiled with other AUTO-07p files.

Python scripts are used to drive AUTO-07p, handle the data set, classify the different families.

Shell scripts relate the array jobs to python files, extract information from the output files, compile AUTO files, libraries and time series integration subroutine.

A batch script is to submit jobs and set rules for them in Sharcnet.

The structures of the mentioned language and software are in Fig. 3.8.
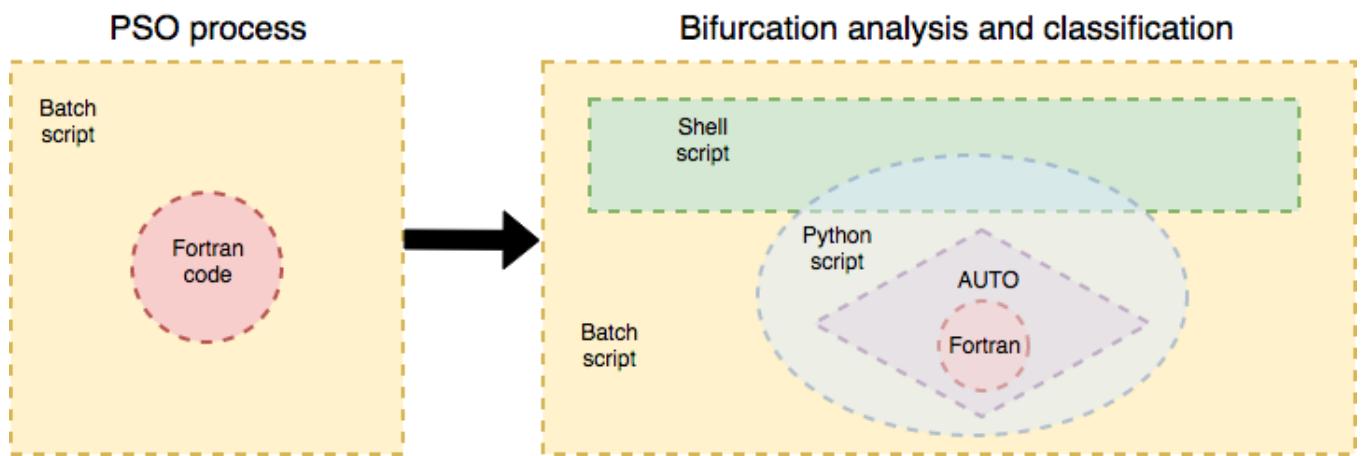
Figure 3.8: Language and software used in the research. The first graph represents the particle swarm optimization process to obtain the raw data, the seond graph represents the bifurcation analysis and the classification process where the interaction between shell script and python script is used to deal with the bifurcation results and classify them into families.

Chapter 4

Implementation

There are three main steps in the implementation part: First, we apply the particle swarm optimization (PSO) method to search the thirteen-dimensional parameter space of the F-K model to gain the parameter sets that can generate the physiologically meaningful one-dimensional ventricular graphs at $T = 700$ms. The second step is to do the bifurcation analysis on parameter sets selected randomly from those meaningful parameter sets. Thirdly, we classify the parameter sets chosen to do the bifurcation analysis into different parent families and subfamilies based on the different qualitative behaviors as T decreases from 700ms to 150ms.

4.1   Hyperbolic Tangent Function

Before we execute those three steps, it is important to make the F-K model differentiable. Here, we introduce sigmoid functions which are mathematical functions having a characteristic "S"$-$shaped curve. Often, a sigmoid function refers to the particular case of the logistic function when the transition area is tiny. A wide variety of sigmoid functions have been used as the activation function of artificial neurons or stimuli, including the logistic and hyperbolic tangent functions[17]. The stepwise function as mentioned in the F-K model can be written as a revised hyperbolic tangent function if k^{step} is large in

Eq.(4.1):

$$\ominus(x_1 - x_2) = \begin{cases} 1 & x_1 \geq x_2 \\ 0 & x_1 < x_2 \end{cases} \approx \frac{1}{2} + \frac{1}{2}\tanh(k^{\text{step}}(x_1 - x_2)) \tag{4.1}$$

where k^{step} is stiffness. when k^{step} is small, the transition from 0 to 1 is relatively slow; in contrast, when k^{step} is large, the transition between 0 and 1 is fast. We use a revised hyperbolic tangent function with $k^{\text{step}} = 500$. If k^{step} is large, the stiffness problem will appear to make Newton's method hard converge. Therefore, we would like to choose a relatively small value for k^{step} as long as the smallest k^{step} still can make dt smaller than any time constant in Table. 2.1. In chapter 4.3.1, we will introduce a relation $dt \leq \tau_r/k^{\text{step}}$ where the maximum value of τ_r is 250ms; therefore the maximum $dt < 0.5$ that is still smaller than all the time constants in Table. 2.1.

4.2 Stimulus Function

Like mentioned, there is an external periodic stimulus current as a pacemaker in the F-K model J_{stim}. It is necessary to create a function to simulate J_{stim}. Essentially, the stimulus is the diffusive current experienced by a cell in a one dimensional cable as the wave propagate down the cable. What has been recorded is the voltage experienced by that cell during a time period. Fig. 4.1 shows the external stimulus data obtained from the numerical data based on the F-K model where the time period is 14ms and the regression line.

According to the behavior of the stimulus-current data, I have created a function that can generate the similar shape with the specific values for parameters:

$$R(t, t_c, a_l, a_r, b_l, b_r) = \frac{-(t - t_c)}{(e^{a_l \cdot t + b_l} + e^{a_r \cdot t - b_r})} \tag{4.2}$$

where t is a variable, t_c, a_l, a_r, b_l and b_r are parameters, we give the initial value to these
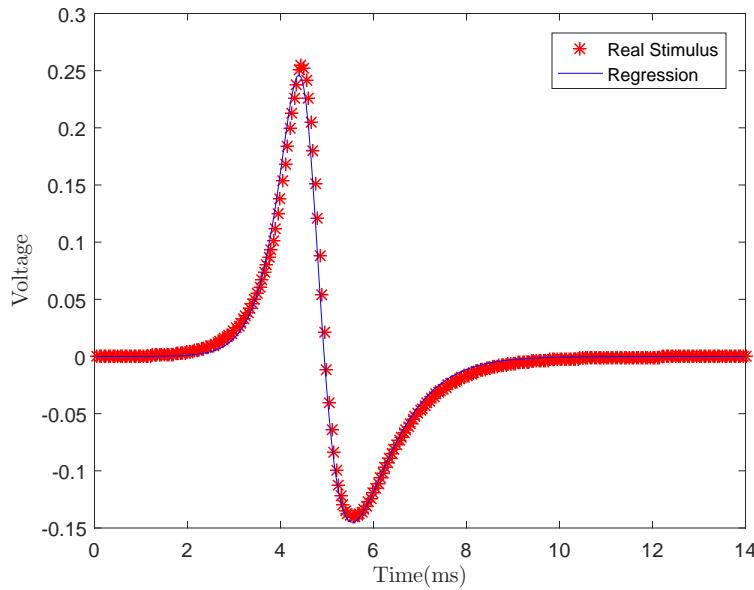
Figure 4.1: Regression of a set of stimulus data. The red stars indicate the external stimulus current recorded every 0.05ms from a numerical data described in the text, and the stimulus lasts 14ms. The blue line is the regression line

parameters and implement Newton's method to get a better approximation of those five parameters.

The function we want to minimize is

$$G(t_c, a_l, a_r, b_l, b_r) = \sum_{t=0}^{t=14} R(t, t_c, a_l, a_r, b_l, b_r) - y(t) \tag{4.3}$$

where $y(t)$ is the experimental data.

After solving $\bigtriangledown G_{pars} = 0$, we get approximate value of those five parameters, and the stimulus function becomes Eq.(4.4) that is used to draw the regression (blue) line in Fig. 4.1.

$$R(t) = \frac{-(t - 4.94)}{\left(e^{-3.09 \cdot t + 14.08} + e^{1.70 \cdot t - 8.03}\right)} \tag{4.4}$$

Eq.(4.4) is a function chosen to represent the external periodic stimulus J_{stim} in the F-K model.

4.3   Time-step integration

The time-step integration is applied in the mentioned first two steps; therefore, we will show the time-step integration. The procedures are in Algorithm.1, and details are explained in the following subsections. Since the first several periods are not stable, we only care about the behavior after t_{trans}, which will be used to compute the score for each parameter set in the PSO process.

Algorithm 1: Time-step integration referred to Chapter 4.3

       input : Initial values $X_0 = (u_0, v_0, w_0)$, parameter set,

       output: Solution $X_{t_{\max}} = (u_{t_{\max}}, v_{t_{\max}}, w_{t_{\max}})$ after n periods

1 $dt=\min(dt, \tau_{\mathrm{r}}/k^{\mathrm{step}})$;

2 for $j \leftarrow 0$ **to** $\mathrm{int}(t_{\max}/dt)$ **do**

3   Implement the trapezoidal rule to solve the nonlinear equations with

        Newton's iteration;

4 $X_{n+1} \leftarrow X_{n+1}^{\mathrm{conv}}$

5   **if** not converge **then**

6   exit;

7   **end**

8   **for** $t > t_{\mathrm{trans}}$ **do**

9   Compute the score for each parameter set in the PSO process;

10   **end**

11 end

4.3.1 $dt = \min(dt, \tau_{\mathrm{r}}/k^{\mathrm{step}})$

We set $dt = 0.05$, however, Newton's iteration cannot converge in some parameter sets.

In Newton's iteration, we have checked the Jacobian matrix:

$$D_{X_{n+1}^i} G(X_n, X_{n+1}^i) = \begin{bmatrix} \partial_{u_{n+1}^i} G(1) & \partial_{v_{n+1}^i} G(1) & \partial_{w_{n+1}^i} G(1) \\ \partial_{u_{n+1}^i} G(2) & \partial_{v_{n+1}^i} G(2) & \partial_{w_{n+1}^i} G(2) \\ \partial_{u_{n+1}^i} G(3) & \partial_{v_{n+1}^i} G(3) & \partial_{w_{n+1}^i} G(3) \end{bmatrix} \tag{4.5}$$

Where the condition number of $\bigtriangledown G$ is too large that results u cannot converge properly, which happens around variable u passes the threshold u_c. As we know,

$$\partial_t u = -J_{\text{fi}}(u; v) - J_{\text{si}}(u; w) - J_{\text{so}}(u) + J_{\text{stim}}(T) \tag{4.6}$$

where

$$J_{\text{fi}}(u; v) = -\frac{1}{\tau_d} v \ominus (u - u_c)(1 - u)(u - u_c) \tag{4.7}$$

$$J_{\text{si}}(u; w) = -\frac{1}{2\tau_{\text{si}}} w(1 + \tanh[k(u - u_c^{\text{si}})]) \tag{4.8}$$

$$J_{\text{so}}(u) = \frac{1}{\tau_o} u \ominus (u_c - u) + \frac{1}{\tau_r} \ominus (u - u_c) \tag{4.9}$$

when u passes u_c, $J_{\text{fi}}(u; v) = 0$ because $u - u_c \approx 0$, $J_{\text{si}}(u; w) = 0$ because u is much smaller than u_c^{si}. The only problem is $J_{\text{so}}(u)$. In chapter 4.1, we rewrite the stepwise function as Eq.(4.10):

$$\ominus(u - u_c) = \begin{cases} 1 & u \geq u_c \\ 0 & u < u_c \end{cases} = \frac{1}{2} + \frac{1}{2}\tanh(k^{\text{step}}(u - u_c)) \tag{4.10}$$

where we set $k^{\text{step}} = 500$. We assume when $u = u_c - \frac{1}{2}k^{\text{step}}$, $\ominus(u - u_c) = 0$; when $u = u_c + \frac{1}{2}k^{\text{step}}$, $\ominus(u - u_c) = 1$; therefore $\triangle u = 1/k^{\text{step}}$ is the value of the hyperbolic tangent function changes from 0 to 1. If there are several time steps in this transition area that can promise Newton's method convergent, $\triangle t$ should be:

$$\triangle t = \frac{\triangle u}{\dot{u}} \tag{4.11}$$

where $\triangle u = 1/k^{\text{step}}$, we take the derivative of $\dot{u}$ with respect to u, we get:

$$\frac{d}{du}\dot{u} = \frac{1}{(2\tau_{\text{r}}(1+(u-u_{\text{c}})^2))} + \frac{u}{(2\tau_o(1+(u-u_{\text{c}})^2))} + \frac{(1+\arctan(u-u_{\text{c}}))}{2\tau_o} \qquad (4.12)$$

where $\frac{d}{du}\dot{u}$ is bigger than 0 when $u_{\text{c}} - \frac{1}{2}k^{\text{step}} \leq u \leq u_{\text{c}} + \frac{1}{2}k^{\text{step}}$, so when $u = u_{\text{c}} + \frac{1}{2}k^{\text{step}}$, we can get the maximum value $\dot{u}_{\max} = 1/\tau_{\text{r}}$; therefore, if $\triangle t$ is smaller than τ_r/k^{step}, there will be some points in this transition area

the smallest time step time $\tau_{\text{r}}/k^{\text{step}}$ can ensure that there are some time steps in the transition area.

4.3.2   Solve nonlinear equations

In each time step, we execute the forward Euler method to compute a fairly good estimate of X_{n+1} that can be used as the initial guess of Eq.(4.13):

$$X_{n+1} = X_n + \frac{1}{2}dt(F(t_n, X_n) + F(t_{n+1}, X_{n+1})) \qquad (4.13)$$

where $X = (u, v, w)$, $F(t, X)$ is the differential equation of u, v and w with respect to t.

In Algorithm.2, we use Newton's method to solve Eq.(4.13) to get a better approximation of X_{n+1} in each iteration.

When the error is smaller than $\text{err}_{\text{toller}} = 10^{-14}$, and the residual is smaller than $\text{res}_{\text{toler}} = 10^{-14}$ before the number of iteration reaches $\text{iter}_{\max} = 10$, Newton's method converges and moves to the next time step; otherwise, exit the time-step integration loop.

4.4   PSO implementation

We have show the F-K model with three variables and thirteen parameters; different parameter sets will have different behaviors in term of (u, v, w).

Algorithm 2: Implement the trapzoidal rule to solve nonlinear ODEs in the

F-K model with Newton's method, referred to Chapter 4.3.2

---

    input : Initial guess X_{n+1}^0

    output: X_{n+1}^{conv}, converge=true .OR. false

1 **for** $i \leftarrow 1$ **to** $\mathrm{iter}_{\max}$ **do**

2   Solving nonlinear equation

$$G(X_{n+1}^i, X_n) = X_{n+1}^i - X_n - \frac{1}{2}dt(F(t_n, X_n) + F(t_{n+1}, X_{n+1}^i)) = 0;$$

3   residual=$||G(X_{n+1}^i, X_n)||$;

4   error=$||X_{n+1}^{i+1} - X_{n+1}^i||$;

5   **if** error $\leq \mathrm{err}_{\mathrm{toler}}$ and residue $\leq \mathrm{res}_{\mathrm{toler}}$ **then**

6   converge=true;

7   **else**

8   converge=false;

9   **end**

10 **end**

11 $X_{n+1}^{\mathrm{conv}} \longleftarrow X_{n+1}^i$;

We implement the PSO process to search parameter space where the domain of each parameter is shown in Table. 2.1. In each PSO step, the score of each parameter set is computed by three criteria and the details are explained in Chapter 4.4.3: 1. the number and the value of peaks of voltage (u) in one period; 2. the stability of the solution; 3. the behavior of the periodical APD restitution curve. After each PSO step, the parameter sets and the corresponding stable solutions are updated. The details of the PSO implementation are shown in the following subsections.

4.4.1 Master-Slave model

To make the PSO process be implemented efficiently and computationally, we apply OpenMP and Open MPI in the PSO procedure to speed up the searching process.

Since OpenMP and Open MPI are the programming interfaces, we create the Master-Slave model as shown in Algorithm 3 to implement this process and search a parameter space as large as possible during the limited time. Master processor assigns different parameter sets to slaves with Open MPI, and slave processors evaluate scores for the parameter sets with OpenMP.

Algorithm 3: Master-Slave model in PSO implmentation referred to Chapter 4.4.1

Result: The parameter sets and the stable solutions with score>0

1 if Initialization of Open MPI returns 0 **then**

2   **if** process ID = 0 **then**

3   Call master processor;

4   **else**

5   Call slave processors;

6   **end**

7 end

In Algorithm 3. There are two output files: The first file includes all meaningful parameter sets and each line shows one parameter set. The second file includes the solution points, and each row show the last solution point of (u, v, w) after ten periods.

Initialization of Open MPI is to check whether the number of processors is larger than two because there must be two processors at least where one is master processor and the other one is slave processor.

Master processor is the stem to initialize data, send the data to slave processors, receive the results from slaves and update the data with the PSO method. On the other hand, slave processors receive the data, compute the time-step integration of the F-K model and the score of the parameter sets; moreover, they send back the results to the master processor to update the data. We will introduce the implementation that the master processor and the slave processors work as follows.

4.4.2   Master processor

Algorithm 4 shows the responsibilities of the master processor by order, and the subroutines are explained concretely.

Subroutine: Initialization

According to Table. 2.1, there are thirteen parameters with their domains. We randomly choose nn $= 10^4$ particles that are the parameter sets according to a uniform distribution between the lower bound and the upper bound in each dimension. In each parameter set, $u_{\mathrm{v}} < u_{\mathrm{c}} < u_{\mathrm{c}}^{\mathrm{si}}$.

Subroutine: Round-robin continuous distribution

The Round-robin method is to allocate nn numbers from 1 to nn to mm groups, the size of each group is either the quotient of nn/mm or the quotient of nn/mm plus 1. Input

---

Algorithm 4: Master processor referred to Chapter. 4.4.2

      output: Two files: one includes the parameter sets and the other one has the

             corresponding stable solutions with scores$>$0

1 while $t < t_{\max}$ **do**

2   Call subroutine: Initialization;

3   Call subroutine: Round-robin continuous distribution;

4   MPI broadcast(Size^i, Initial position (u_0, v_0, w_0));

5   **for** $i \leftarrow 1$ **to** np (outer) **do**

6   Master sends data to slave processors;

7   Master receives results from slave processors;

8   Call subroutine: Global best;

9   Call subroutine: PSO updating;

10   **for** $j \leftarrow 1$ **to** nn **do**

11   Compute the distance between the previously recorded parameter

                 set and the current parameter set with the same index;

12   **if** dist $>$ dist$_{\min}$ **then**

13   Write the updated score, parameter set and the corresponding

                    stable solution (u, v, w) into disk;

14   **end**

15   Compute the mean distance between the center of the particles and

                 all the particles.;

16   **if** Mean$_{\text{dis}}$ $<$ Mean$_{\min}$ **then**

17   exit outer ;

18   **end**

19   **end**

20   **end**

21 end

22 Call subroutine: Stop slaves

---

is the total index number n and the number of groups mm, and output is the first index and the last index in each group. The size of the group is:

$$\text{Size}^{\text{i}} = \text{Index}^{\text{i}}_{\text{last}} - \text{Index}^{\text{i}}_{\text{first}} + 1 \tag{4.14}$$

We use the Round-robin method to allocate nn $= 10^4$ parameter sets to mm $= 31$ slave processors; therefore, each slave processor i will only compute its parameter sets from $\text{Index}^{\text{i}}_{\text{first}}$ to $\text{Index}^{\text{i}}_{\text{last}}$ in the whole PSO process, and the number of parameter sets is either 332 or 323.

Master broadcasting, sending and receiving

In Master broadcasting, the master processor sends out the same initial value $X_0 = (0, 1, 1)$ and tell mm $= 31$ slave processors to take their own parameter sets.

In each PSO step, the master processor sends the parameter sets needed to be computed between $\text{Index}^{\text{i}}_{\text{first}}$ and $\text{Index}^{\text{i}}_{\text{last}}$ to the slave processor (i) and the local best parameter sets also need to be updated where a updated local best location is the one with a higher score between the previous local best position and the current position in each parameter set. The data received by the master processor is the updated local best parameter sets, the parameter sets with the computed scores and the corresponding stable solutions after ten periods.

Subroutine: Global best

The global best parameter is to set the parameter set with the highest score among all the local best parameter sets in each PSO step.

Subroutine: PSO updating

This subroutine is based on the PSO procedure shown in Eq.(4.15) where we set inertia weight $\omega = 0$. The details of the PSO process are in Chapter. 3.2.

$$P_{ij}^{t+1} = P_{ij}^t + R_1 d_s (LP_{ij}^t - P_{ij}^t) + R_2 d_s (GP_i^t - P_{ij}^t) \tag{4.15}$$

where i is the index of thirteen parameters, j is the index of the parameter set, LP is the local best parameter set, GP is the global best parameter set among all the local best parameter sets, $ds = 0.1$ is the step size, and R_1 and R_2 are the random numbers between 0 and 1 according uniform distribution.

There are two new rules in the PSO updating procedure: First, each updated parameter value in one parameter set must be in its domain; otherwise, that parameter will not be updated, but the other parameters can be updated in that parameter set. Second, the updated values for u_v, u_c, u_c^{si} must obey $u_v < u_c < u_c^{si}$; otherwise, they have to keep the previous values, but the rest of parameters in the problematic parameter set, can be updated.

Distance and mean distance

After each PSO step, all parameter sets are updated and some parameter sets have the score bigger than 0. However, there is a problem when some updated particles are very close to their previous position, and both have the score bigger than 0. As a result, the previous and current parameter sets have the similar information, and we do not want to record this redundant information; therefore, we only keep the previous parameter set and the corresponding solution in disk until the updated parameter set is not very close to the previous one; then, we write the new parameter set into disc.

The distance between the current position and the previous position of the same particle can estimate the difference with respect to the information they include. The normalized distance is given by Eq. (4.16).

$$\text{Distance} = \sqrt{\sum_{i=1}^{i=13} \left(\frac{P_{curr}^i - P_{prev}^i}{\text{Bound}_{up}^i - \text{Bound}_{low}^i} \right)^2} \tag{4.16}$$

where i is the index of thirteen parameters, Bound_{up} and $\text{Bound}_{\text{low}}$ are the domains of parameters. When the distance between the previous position and the current location is larger than the minimum distance ($\text{dist}_{\text{min}} = 0.01$), we add the current parameter set as new information.

Furthermore, there is another problem: All particles are updated according to the local best parameter sets, the global best parameter set and the random force. One of the local best parameter sets is the global best parameter set. If there is one parameter set with an unexpectedly high score, this parameter set will never be updated according to Eq.(4.15). Therefore, that particle will always be the global best parameter set in the whole PSO process, and all other particles will swarm to the position of that particle. However, our goal is not to optimize the function to find the best solution. Instead, we want particles to search locally rather than convert to the global best position. In order to avoid this problem and accomplish our goal, we compute the mean distance between the center of particles and all particles shown in Eq.(4.17):

$$\text{Mean}_{\text{dis}} = \frac{1}{n} \sum_{i=1}^{i=n} \sqrt{\sum_{j=1}^{j=13} \left(\frac{P_i^j - 1/n \sum_{k=1}^{k=n} P_k^j}{\text{Bound}_{\text{up}}^j - \text{Bound}_{\text{low}}^j} \right)^2} \qquad (4.17)$$

where $1/n \sum_{k=1}^{k=n} P_k^j$ is the center of all the particles.

If the mean distance is smaller than the minimum mean distance set as $\text{Mean}_{\text{min}} = 0.1 * \sqrt{13}$, we consider that all particles are too close to each other that will result in the searching procedure stalling. Therefore, we will stop the PSO procedure, go back to reinitialize n particles with a different random seed and restart a new PSO procedure until the time reaches the maximum (15 days). In our implementation, when t reaches t_{max}, there are 33 times that the PSO process has been restarted.

4.4.3   Slave processor

After introducing the master processor as a stem of the PSO procedure, let us look at how slave processors work in Algorithm 5.

Master processor broadcasts the same initial value $X_0 = (0, 1, 1)$ to all slave processors; nevertheless, the initial value is not the stable solution of each parameter set; hence, we compute 10 cycle lengths to acquire a stable solution point for each parameter set. Moreover, after integrating 10 cycle lengths for each parameter set, we can gain the relatively consistent behavior that can be used to record APDs and peaks to evaluate the score.

Algorithm 5: Slave processor (Size_i is explained in Algorithm 4) referred to Chapter 4.4.3

---

      input : Parameter sets from the first index to the last index and the local

             best parameter sets

    output: Parameter sets with their computed scores and the updated local

             best parameter sets with their scores

1 **while** Receiving tag $\neq$ Exit tag **do**

2   Slave processor receive data from master processor;

3   Begin OpemMP parallel structure;

4   **for** $j \leftarrow 1$ **to** Size_i **do**

5   Call subroutine: Peak, APDs and Stable solutions;

6   Call subroutine: The score of the parameter set;

7   **end**

8   End OpenMP parallel structure;

9   Call subroutine: Local best;

10   Salve processor sends back the results to master processor;

11 **end**

Slave processors receiving and sending

Exit tag forwarded by master processor is the signal to stop slave processors when the time is finished. The slave processors receive the parameter sets needed to be computed and the local best parameter sets ready to be updated. The results sent by the slave processors include the parameter sets with the scores, the updated local best parameter sets with the scores, and solutions.

Begin and end OpenMP

Since time-step integration is independent and time-consuming, we use "!$omp parallel private()" and "!$omp do" commands to implement a parallel structure in each node with 16 threads, which will speed up the computing process in each slave processor around 16 times faster than the processor with only one thread.

Subroutine: Peak, APDs and Stable solutions

In Algorithm 6, we integrate 10 cycle lengths and consider the end of transient time is 8th cycle length. The implementation of the time-step integration is explained at the beginning of this Chapter. During the ten periods, we compute and record the information that we need for estimating the score for each parameter set.

Subroutine: Peak

In the F-K model, there is only one peak of u in each period between depolarization and repolarization. We record X_t as the peak value ($X_{\max}$) in one period if $X_{t-dt} < X_t$ and $X_t > X_{t+dt}$, and the number of $X_{\max}$ appearing as the number of peaks in that period.

Subroutine: The score of the parameter set

In Algorithm 7, we compute the scores for parameter sets based on the number of peaks, the value of peaks, APDs and the stability of the periodic behavior.

Algorithm 6: Peak, APDs and Stable solutions referred to Subroutine: Peak,

APDs and Stable solutions

---

    input : Initial vales $X_0 = (0, 1, 1)$, parameter set,

    output: Stable solution, the number of peaks, peak value, APDs in the last

            two periods

1 for $t \leftarrow 0$ **to** *10* periods **do**

2 $t_{\text{trans}} = 8$ cycle lengths;

3   **if** $t \leftarrow$ 8th period **to** 9th period **then**

4   Call subroutine : Peak;

5   **if** $u \geq u_{\text{c}}$ **then**

6 $\text{APD}_9 = +dt$;

7   **end**

8   **end**

9   **if** $t \leftarrow$ 9th period **to** 10th period **then**

10   Call subroutine : Peak;

11   **if** $u \geq u_{\text{c}}$ **then**

12 $\text{APD}_{10} = +dt$;

13   **end**

14   **end**

15 end

Algorithm 7: Compute Score referred to Subroutine: The score of the parameter set

    input : APDs, peaks and parameter set

    output: Score

1 Score=0;

2 **if** $\mathrm{APD_l} \leq \mathrm{APD_9}, \mathrm{APD_{10}} \leq \mathrm{APD_u}$ **then**

3   **if** $\mathrm{npeak_9}, \mathrm{npeak_{10}} = 1$ **then**

4   **if** $\mathrm{Peak_l} \leq \mathrm{Peak_9}, \mathrm{Peak_{10}} \leq \mathrm{Peak_u}$ **then**

5   **if** $\parallel \mathrm{Peak_9} - \mathrm{Peak_{10}} \parallel \leq 0.1(\mathrm{Peak_u} - \mathrm{Peak_l})$ **then**

6   Compute score by Eq.(4.18);

7   **end**

8   **end**

9   **end**

10 **end**

In Algorithm 7, APD_9 and APD_{10} are the action potential durations in the last two periods; $APD_l = 175ms$ and $APD_u = 425ms$ are the bounds of APDs. $Peak_l = 1.05$ and $Peak_u = 1.35$ are the bounds of peak values[2][9].

First, APDs must be in the domain between APD_l and APD_u; otherwise, the score is 0. Second, there must be only one peak in each period; if not, Score = 0. Moreover, the peak value must be in the domain from $Peak_l$ to $Peak_u$; otherwise, the score still equals 0. Furthermore, $\| Peak_9 - Peak_{10} \| \leq 0.1(Peak_u - Peak_l)$ is to check the stability of the periodical solution; if the distance between the last two peaks is bigger than 10% of the distance between $Peak_l$ and $Peak_u$, Score = 0. Finally, if the parameter set can satisfy all the criteria mentioned above, we can compute the quantitative score through Eq. (4.18)

$$Score = \max(1 - 2 \| APD_{10} - (APD_u + APD_l)/2 \| /(APD_u - APD_l), 0) \qquad (4.18)$$

where the score is computed based on the distance between APD_{10} and the mid-value between APD_l and APD_u, and the maximum score is 1 and the minimum score is 0.

Subroutine: Local best

This subroutine is to compare two scores between the local best position and the current position of one particle. The position with a higher score will be chosen as the updated local best position for that particle.

4.5   Bifurcation analysis in AUTO

After applying the PSO process in searching the parameter space of the F-K model, we have tested more than 200 million parameter sets and obtained around 1.5 million parameter sets having scores bigger than zero; simultaneously, we have recorded the corresponding solutions for each parameter set at $T = 700ms$.

In the PSO implementation, we set $T = 700$ms that is a relatively slow pacing speed of the human heart, and we get a repetitive stable behavior for those 1.5 million parameter sets or so. Then, we increase the pacing frequency from $T = 700$ms to $T = 150$ms per beat and observe where the behavior changes qualitatively. The method we use to monitor the behavior changing is bifurcation analysis.

We have done the bifurcation analysis on the F-K model 270,000 parameter sets selected randomly from those 1.5 million sets where the control parameter is T varying from 700ms to 150ms that can be considered as a physiologically rapid heartbeat.

4.5.1 AUTO: bifurcation code

We ask AUTO to do the bifurcation analysis. AUTO has two functionalities. The first one is aimed at solving the continuous solutions of the systems of ordinary differential equations (ODEs); the second one is to perform limited bifurcation analysis of algebraic problems in a discrete system. [7]

We design the system as a Poincaré map that can be interpreted as a discrete dynamical system; therefore, we choose the code in the second family in AUTO to do the bifurcation analysis.

4.5.2 AUTO: Bifurcation analysis

According to Chapter 3.1 and Chapter 4.3, we know how to solve the linearized ODEs and nonlinear ODEs of the F-K model. In Algorithm 8, the input is initial value X, and we implement the time-step integration after one period to obtain output $\phi(X, T)$.

We would like to solve Eq.(4.19) to find the numerical approximation of the fixed point $Z = (X, T)$ when the control parameter T varies.

Algorithm 8: Poincaré map (ϕ explained in Chapter 3.4.1) referred to Chapter 4.5.2

---

    input : X_0, T,

    output: $\phi(X,T)$, $D_X\phi(X,T)$, $D_T\phi(X,T)$, APD

1 APD=0;

2 while $t \leq T$ **do**

3   Solve the nonlinear ODEs of the F-K to get X_t in each time step. Details are in Chapter 3.1 (Eq.(3.4)) and Chapter 4.3.2 (Eq.(4.13));

4   Solve the linearized ODEs of the F-K to obtain $D_X\phi(X,t)$ in each time step. Details are in Chapter 3.1 (Eq.(3.5) and Eq.(3.9)) ;

5   **if** $u \geq u_c$ **then**

6 $APD = +dt$;

7   **end**

8 $\phi(X,t)=X_t$;

9 $t = t + dt$;

10 end

$$G(X, T) = \phi^p(X, T) - X = 0$$

$$\psi(X, T) = 0 \tag{4.19}$$

where $\psi(X, T)$ is the phase condition given by AUTO. Details are shown in Chapter 3.4.2.

AUTO uses Newton's method to solve Eq.(4.19) to gain a successively better approximation of the fixed point Z. The details are shown in Eq.(4.20)

$$\begin{bmatrix} D_X G & D_T G \\ D_X \psi & D_T \psi \end{bmatrix} \begin{bmatrix} \delta X \\ \delta T \end{bmatrix} = - \begin{bmatrix} G \\ \psi \end{bmatrix} \tag{4.20}$$

where δX and δT compose a error vector; when $\| \delta X \| <$ EPSU, $\| \delta T \| <$ EPSL, Newton's method converges. In AUTO, EPSL and EPSU are the convergence criterion for equation parameters and equation variables in Newton's method, and the values are in Table. 4.1.

In Eq.(4.20), $D_T G = D_T \phi(X, T) = (\dot{u}, \dot{v}, \dot{w})$ at $t = T$ and $D_X G$ are the output in Algorithm 8. $D_X \psi$ and $D_T \psi$ are computed by AUTO.

We can get $D_X \phi(X, T)$ after one period T, and $D_X G = D_X \phi(X, T) - I$. Then we can solve Eq.(4.20) with Newton's iteration to obtain the solution curve as control parameter T varies.

When one of the eigenvalues of $D_X G$ passes 1, AUTO will record that value for T as a fold bifurcation; similarly, as one of the eigenvalues of $D_X G$ passes -1, the point is recorded as a period doubling bifurcation.

4.5.3   AUTO: setting

There are several important setting parameters we need to introduce in AUTO: 1. unames=$(1 : "u", 2 : "v", 3 : "w")$ are the variables. 2. paranames=$(1:"T", 2:"APD")$ where T is the control parameter and APD is the output parameter. 3. ISW=1 is the

Table 4.1: Values for parameters in Bifurcation Analysis in AUTO (See Chapter 4.5.3 for the meaning of the parameters)

Parameter	Range(ms)	Parameters	Range(dimensionless)
EPSL	10^{-6}	EPSU	10^{-6}
EPSS	10^{-4}	ITMX	10
DS	-0.5	DSMIN	-10^{-13}
DSMAX	-1		

normal value; however, ISW=-1 is the label to switch the branch to trace another solution from the period-doubling bifurcation point. 4. EPSS is the relative arclength convergence criterion for the detection of special solutions. 5. ITMX is the maximum number of iterations of Newton's method. DS is the pseudo-arclength where it can adjust from DSMIN to DSMAX. The values of parameters as mentioned above are shown in Table. 4.1.

4.5.4   AUTO: output

There are three output files in AUTO: "Run$_{\text{index}}$.b", "Run$_{\text{index}}$.d", "Run$_{\text{index}}$.s". "Run$_{\text{index}}$.b" includes solutions and APD values corresponding to different T that can be used to draw a bifurcation diagram APDs vs T. "Run$_{\text{index}}$.d" includes all detailed information, and parameter IID controls the volume of output including Jacobian matrix, eigenvalues, residual vectors of variables and parameters and so on. "Run$_{\text{index}}$.s" is a solution file that includes solutions, labels and T values at special points, which can be used to switch branches.

4.5.5 Problem: Two Special Points

When AUTO switches branches, one eigenvalue of Jacobian matrix passes -1 recorded as a period-doubling bifurcation point; however, there are a few cases that two eigenvalues passing -1 at the same T value, the condition number of the Jacobian matrix becomes really big because Newton's iteration becomes divergent, and the output of X and T are not a number anymore. AUTO can not compere a number with a NaN; therefore, AUTO is stuck in one parameter set, and the computation will access to the infinite. If this situation happens, we want AUTO to skip this parameter set and read the next parameter set to do the bifurcation. Therefore, we set the maximum tolerance of error $\text{err}_{\max} = 1$ in Newton's method in the AUTO file, when the error is bigger than the maximum tolerant error. AUTO will exit Newton's loop and output "not convergence result". Then, AUTO will skip the problematic parameter set and continue the bifurcation analysis on the next parameter set.

4.6 Classification

According to the bifurcation graphs, when T decreases from 700ms to 150ms, there are three kinds of stables solutions: One to one solution that means each stimulus initiates an identical response. Two to two alternating solution that represents every other stimulus can excite the same reaction. The two to one blocking solution means that two stimuli only can generate one response; In other words, the second stimulus happens when the ventricular cell that has not recovered yet so it cannot excite another new response.

Algorithm 9 shows the procedure of classifying those 270 thousand parameter sets into parent families and categorize parameter sets with only one period-doubling bifurcation into subfamilies based on the bifurcation patterns shown in Chapter 5.2.

Algorithm 9: Classification of parent families and subfamilies referred to

Chapter 4.6.1

---

    input : Parameter sets, corresponding stable solutions, job array ID

    output: Five parent families

1 **for** $\text{ID}_{\text{Arr}} \leftarrow 0$ **to** ID_{max} **do**

2   **for** $i \leftarrow \text{Index}_{\text{first}}^{\text{ID}_{\text{Arr}}}$ **to** $\text{Index}_{\text{last}}^{\text{ID}_{\text{Arr}}}$ **do**

3   Read parameter set;

4   Read stable solution;

5   AUTO: Bifurcation analysis on the F-K model;

6   Classify P_i into the right parent family;

7   **end**

8   **for** $j \leftarrow 0$ **to** n_{PF2} **do**

9   Read(Parameter set);

10   Read(Stable solution);

11   AUTO: Bifurcation analysis with switching branches on the F-K model;

12   Classify(P_j) into the right subfamily;

13   **end**

14 **end**

4.6.1   Classification based on AUTO results

Because bifurcation analysis on parameter sets is independent, we submit the identical jobs that take different chunks of parameter sets obtained from the PSO process to do the bifurcation analysis. In Algorithm 9, ID_{Arr} is the job ID that we submit to a shared computer where these jobs are independent to each other and have their own memory. According to the memory limitation, we ran 300 independent jobs for 10 days, and each job includes 900 parameter sets. Each array will read different parts of data including the parameter sets and the corresponding stable solutions at $T = 700$ms to do the bifurcation analysis as T varies and classify the parameter sets into five parent families. The categorization for parent families is based on the period-doubling bifurcations, which are shown in Chapter 1.4. If there is not a period-doubling bifurcation, the parameter set belongs to PF1. The parameter set, with one period-doubling bifurcation, belongs to PF2. If there are two period-doubling bifurcations, the parameter set is in PF3; If there are three period-doubling bifurcations, the parameter set belongs to PF4. The parameter sets with convergence problems or more than three period-doubling bifurcations are in PF5.

In each job array, after classifying 900 parameter sets into five parent families, it will continue to read the parameter sets that belongs to PF2 to redo the bifurcation from $T = 700$ms to 150ms and switch branches at the period-doubling bifurcation to trace another solution.

The details of the sub-classification in PF2 are shown in Chapter 1.4. F1 does not have any bifurcation after switching branches. F2 only has the decreasing fold bifurcation after switching branches; F3 has the decreasing fold bifurcation, the increasing fold bifurcation; other parameter sets belong to F4.

After doing the bifurcation analysis, all solutions at the special point are recorded in "$run_{index}.s$" where different special points have different labels. Based on the specific labels such different types of bifurcations, beginning and terminal points, we use bash

commands: "grep" and "wc" to extract the rows with different labels. After counting the number of the rows, we can classify the parameter sets into right parent families and subfamilies.

Chapter 5

Results

5.1 Distributions and Relations

As the result of the PSO process, a collection of 1,525,833 physiologically meaningful parameter sets from more than 200 million is available and considered in this study as a representative sample of physiologically realistic activities of ventricular cells in the F-K model. The rest parameter can not generate the physiological behavior since the nonlinear relations among parameters are not satisfied. In the PSO implementation, we randomly chose values for each parameter from a uniform distribution in their intervals at the beginning, and the intervals for thirteen parameters were from Table. 2.1. After implementing the PSO process, we would like to know the distributions of those thirteen parameters.

From Fig. 5.1, the distributions of parameters are not uniform anymore. Some parameters have really similar skewed distributions, like τ_{v1}^-, τ_{v2}^- and τ_o; in contrast, some distributions of parameter values are opposite skewed such as τ_{si} and τ_w^+.

It is essential to find whether there are some linear relations among the thirteen parameters. We use the Pearson correlation coefficient to detect the linear relations. The Pearson correlation coefficient that is a measure of the strength and direction of the
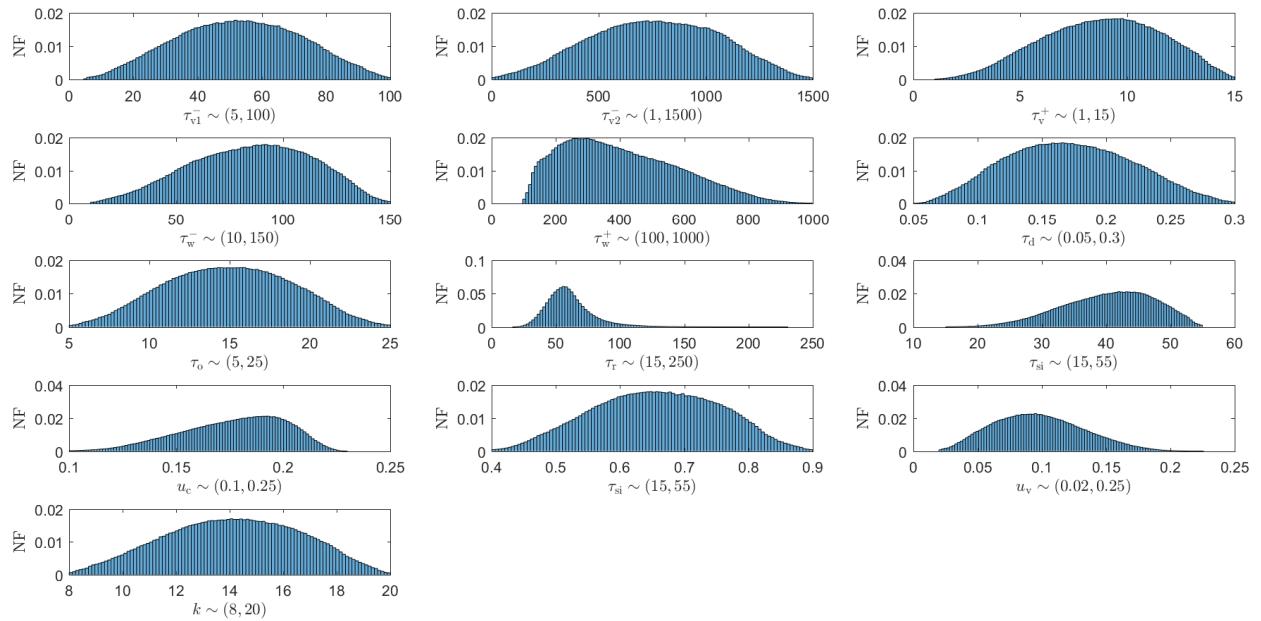
Figure 5.1: Distributions of thirteen parameters The normalized frequencies of thirteen parameter values for the analyzed 1,525,833 sets considered as the physiologically meaningful parameter sets. The number of bins is 500 in each graph

linear relationship between two variables that is defined as the covariance of two variables

divided by the product of their standard deviations[1]:

$$\rho_{ij} = \frac{\sum_{h=1}^{h=n_{\text{tolt}}}(P_i^h - \overline{P_i})(P_j^h - \overline{P_j})}{\sqrt{\sum_{h=1}^{h=n_{\text{tolt}}}(P_i^h - \overline{P_i})^2}\sqrt{\sum_{h=1}^{h=n_{\text{tolt}}}(P_j^h - \overline{P_j})^2}} \tag{5.1}$$

where n_{tolt} is the number of observations and equals 1,525,833. i and j are the index of

thirteen parameters.

According to Table. 5.1, there is a strong linear relation between τ_{r} and τ_{si}. τ_{r}

controls the slow outward currents I_{so} that is responsible for the repoarization of the

membrane; in contrast, τ_{si} is a parameter to control the slow inward currents I_{si} that

balances I_{so} during the plateau phase of the action potential durations [11]. Therefore,

there is a positive linear relation between τ_{r} and τ_{si}. There is also a moderate negative

linear relation between τ_{r} and τ_{w}^+ as a similar reason that τ_{w}^+ controls the slowing gating

variable (w), and the slow gating variable (w) controls I_{si} like τ_{si}.

To see whether it is possible to reduce the number of effective parameters, we have im-

plemented the principal component analysis (PCA) over the number of 1,525,833 param-

eter sets. The result is illustrated in Fig. 5.2, the percentage of total variance explained

by thirteen principal components is plotted, individually and cumulatively. Primarily,

if the parameter space present strongly linear correlations among the variables, it will

be possible to identify a limited number of components capturing the majority of the

variance, indicating that the number of significant parameters were much less than total

number of dimensions.

According to Fig. 5.2, the thirteen components cumulatively account for the total

variance with low and very similar singular contributions. Therefore, we can not find a

linear combination of parameters that express all properties of the parameter space.

	τ_{v1}^{-}	τ_{v2}^{-}	τ_{v}^{+}	τ_{w}^{-}	τ_{w}^{+}	τ_{d}	τ_{o}	τ_{r}	τ_{si}	u_{crit}	u_{c}^{si}	u_{v}	k
τ_{v1}^{-}	1												
τ_{v2}^{-}		1											
τ_{v}^{+}			1										
τ_{w}^{-}				1									
τ_{w}^{+}					1			-0.55					
τ_{d}						1							
τ_{o}							1						
τ_{r}								1	0.80				
τ_{si}									1				
u_{crit}										1			
u_{c}^{si}											1		
u_{v}												1	
k													1

■ strong correlation   ■ moderate correlation   ■ week correlation   no correlation

Table 5.1: Pearson correlation coefficients (ρ) of parameters. The number in the grid shows the correlation between two parameters where the correlation coefficient is from 0 to 1. The pink grid shows the strong linear relation between two parameters, where $0.8 < \rho \leq 1$, the blue grid shows the moderate linear relation between two parameters, where $0.5 < \rho \leq 0.8$, the green shows the week correlation where $< 0.3 < \rho \leq 0.3$ and the blank grind shows very weak or no correlations, where $0 \leq \rho \leq 0.3$.
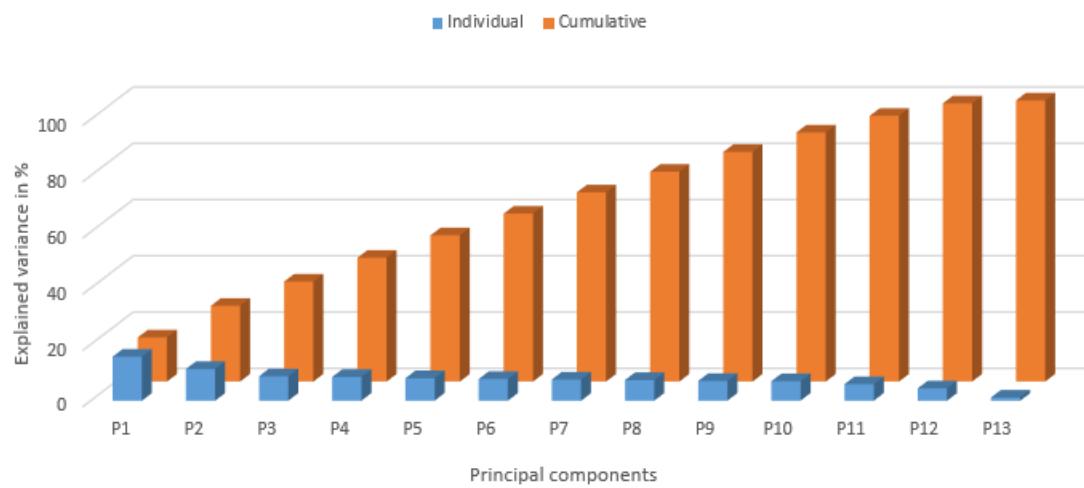
Figure 5.2: Principal Component Analysis of the model parameter space. The fraction of total variance of parameters is explained by the thirteen principal components for 1,525,833 parameter sets. Blue bars indicate individual contributions; orange ones represent their cumulative sum. The evident absence of strong linear correlations within parameter sets means parameter space cannot be reduced easily to a lower number of effective degrees of freedom.

5.2 Classification and Bifurcation diagram

If we want to extract the valuable statistical information, a different, non-standard method of analysis is needed for which we choose bifurcation analysis. We have done the bifurcation analysis on 270 thousand sets selected randomly from the global batch, 1,525,833 parameter sets. By drawing the bifurcation plots, we are guided by the existence of literature pointing to the electric dynamical responses of ventricular cells to the pacing frequency. For instance, the forcing period (T) representing the pacing frequency can be considered as an important parameter, and the periodic APD restitution curves can be the response.

After doing the bifurcation analysis, we can draw and analyze the bifurcation plots visually and numerically. The parameter sets are first classified into five "Parent Families" based on the number of period-doubling bifurcations:

• PF1 has all the parameter sets without any period-doubling bifurcation point, and one example from PF1 is shown in Fig. 5.3. When the pacing frequency is increasing, the solution is always a stable one to one solution until the pacing frequency reaches the minimum value 150ms.

• The parameter sets with only one period-doubling bifurcation are partitioned into PF2, and one example is in Fig. 5.4. Before the period doubling bifurcation occurs, the solution is stable one to one solution; if the pacing frequency continuously increases after the period-doubling bifurcation, the stable one to one solution becomes unstable. The details will be discussed in the sub-classification.

• The parameter sets with two period-doubling bifurcation points are in PF3; Fig. 5.5 is an example in PF3. Before the first period-doubling bifurcation occurs, the solution is stable one to one solution. Then the stable one to one solution becomes unstable; the stable solution bifurcate to a two to two alternating solution or two to one blocking solution after label 2 in Fig. 5.5. When the second period-doubling occurs, the solution bifurcates to stable one to one solution again.
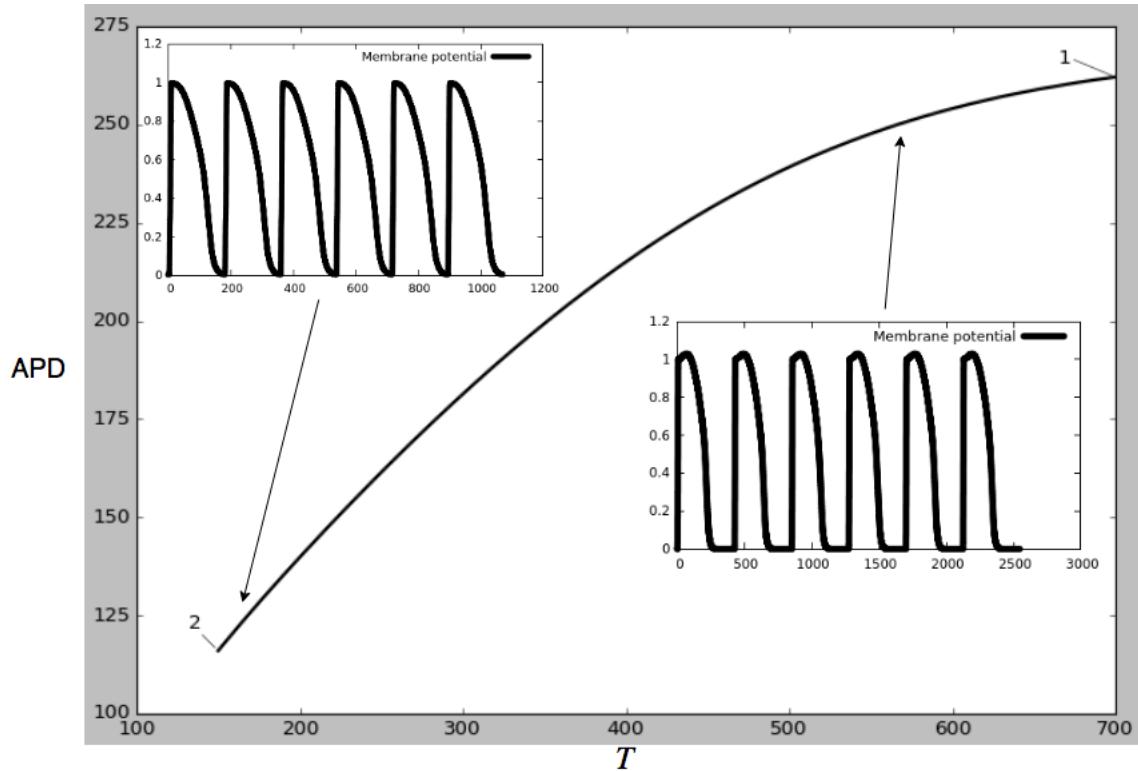
Figure 5.3: Continuation in T of one parameter set in PF1. The interval $150\text{ms} \leq T \leq 700\text{ms}$ is considered as physiologically meaningful pacing time. The black line represents stable equilibria. Label 1 denotes the beginning of the continuation; label 2 is the end of the continuation.
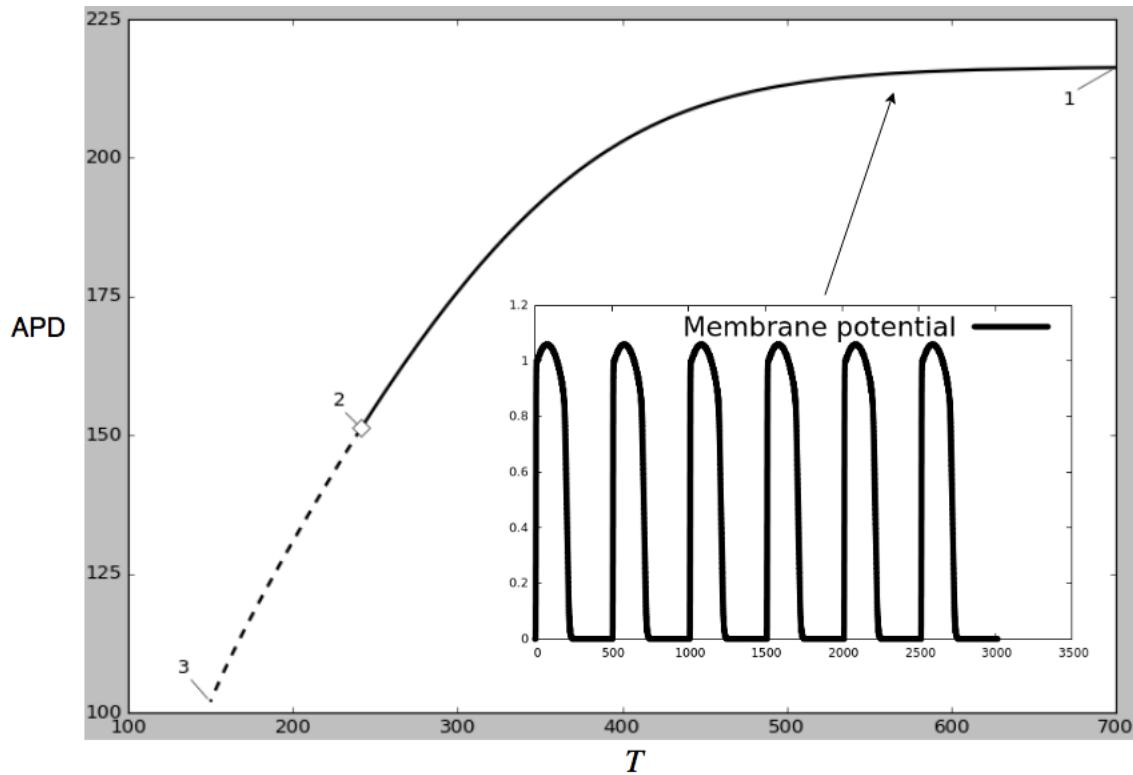
Figure 5.4: Continuation in T of one parameter set in PF2. Label 1 denotes the beginning of the continuation; label 2 is the period-doubling bifurcation point; label 3 is the end of the continuation.
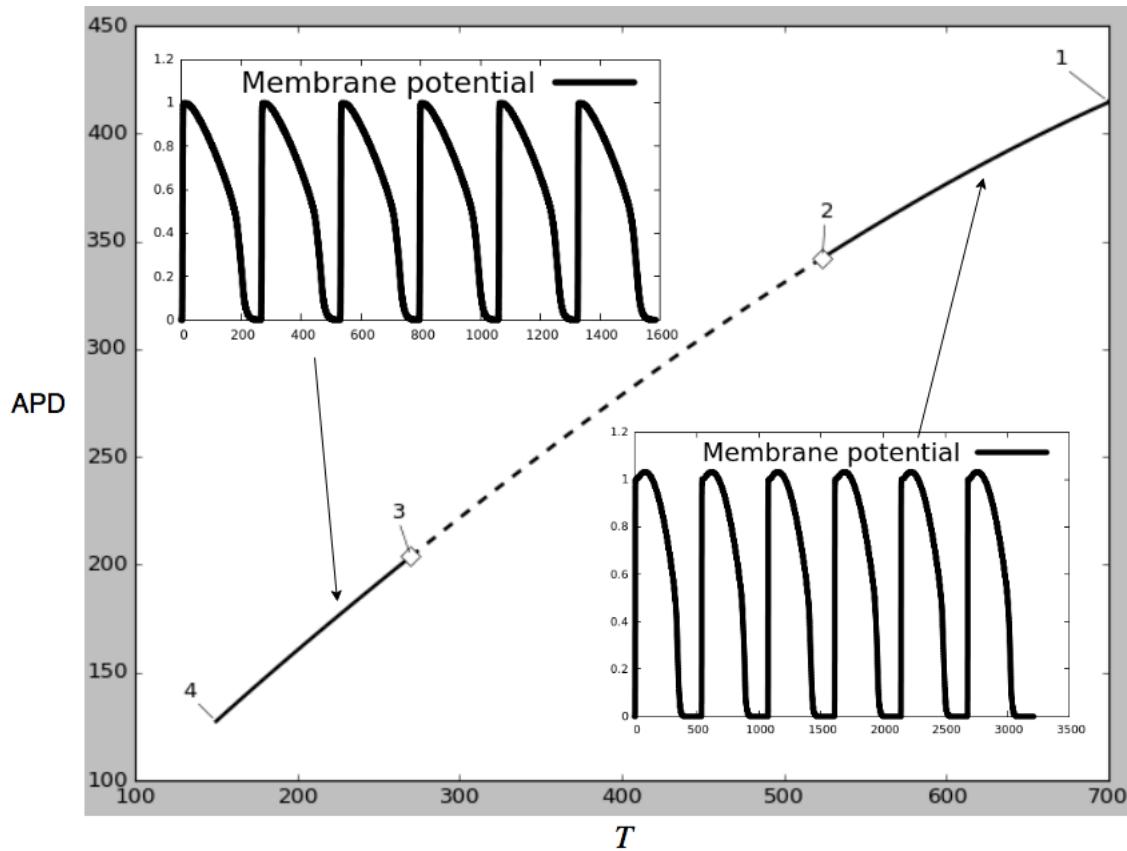
Figure 5.5: Continuation in T of one parameter set in PF3. Label 1 shows the beginning of the continuation; label 2 indicates the first period-doubling bifurcation point; label 3 is the second period-doubling bifurcation; label 4 indicates the end of the continuation.
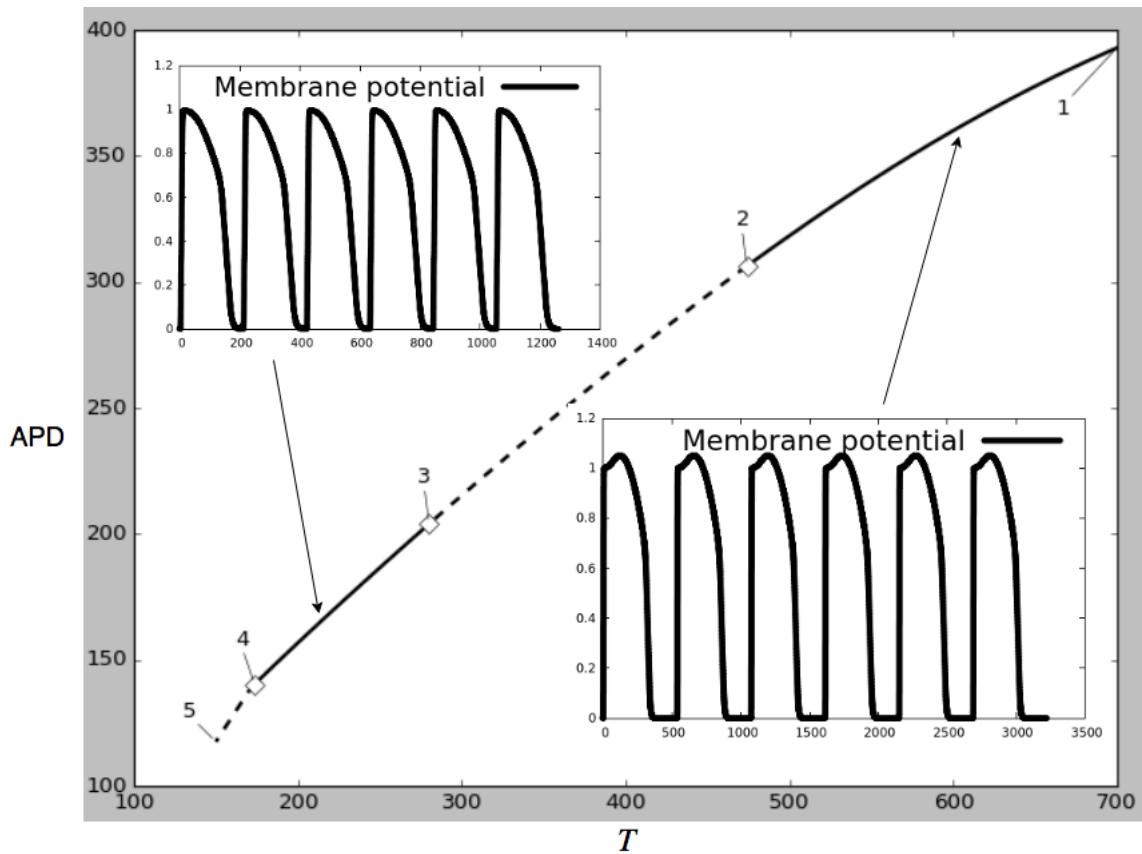
Figure 5.6: Continuation in T of one parameter set in PF4. Label 1 indicates the beginning of the continuation; label 2 is the first period-doubling bifurcation point; label 3 is the second period-doubling bifurcation; label 4 shows the third period-doubling bifurcation; label 5 is the end of the continuation.
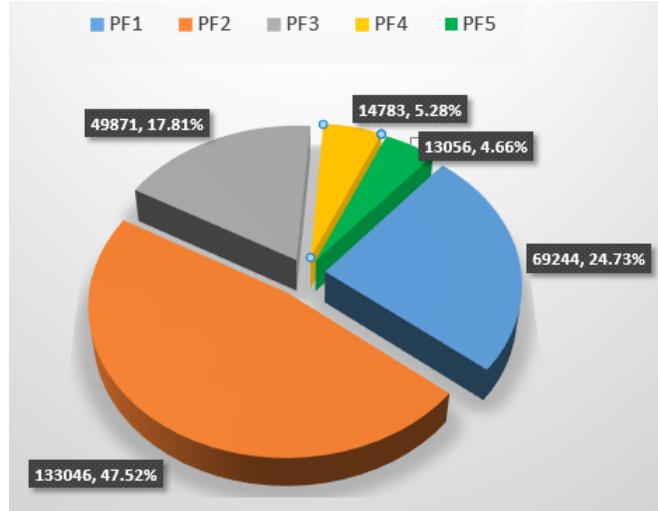
Figure 5.7: Percentage and the number of five parent families The total number is 270 thousand parameter sets. The blue part is PF1,the orange one is PF2; the gray one is PF3, the yellow part belongs to PF4, the green one is PF5.

- PF4 includes all parameter sets with three period-doubling bifurcation points, and one example is in Fig. 5.6. The behavior of one example in PF4 is similar as that of the example in PF3 until the third period-doubling bifurcation appears; after the third period-doubling bifurcation appears, the stable one to one solution becomes unstable again.

- PF5 has the parameters sets with more than three period-doubling bifurcation points, or the continuation performed by AUTO cannot converge as T decreases from 700ms to 150ms. There are a few parameter sets that have five or six period-doubling bifurcations. However, the fifth and sixth period-doubling bifurcation points are close to each other, which means even there is a stable solution between those two bifurcations, it exists for a short interval of cycle lengths. The percentage of these five parent families are in Fig 5.7. We can also tell PF5 only occupies 4.56%

To know how the qualitative behaviors change, we have to switch branches at the period-doubling bifurcation points and trace the solutions along a new branch. In my research, branch switching has not been done in all parent families. There are three

reasons: First, there are different diagrams in PF3, PF4 and PF5. Second, there exist convergence problems. 3. PF3, PF4 and PF5 only occupy less than 28%. Based on Fig. 5.7, PF2 and PF1 are more than 70%. Regarding PF1, there is not even one bifurcation point, so we do not need to switch branches to trace another solution. As for PF2, it occupies the largest percentage (47.52%). Therefore, the second step is to switch branches at the period-doubling bifurcation in PF2 to see the qualitative behaviors and classify PF2 into four subfamilies.

Examples of the continuation are depicted in Figs. 5.8∼5.11, obtained from the batch of 133,046 sets in PF2. We want to stress that the variations within each subfamily are extensive: the plots proposed are only schematic indications and are not meant to exhaustively describe the behaviors of F1, F2 or F3 types. Nonetheless, some general conclusions can be drawn based on the most commonly appearing dynamical traits in the continuation in T.

In F1, we can tell from Fig. 5.8, after switching branches at the period-doubling bifurcation point, the stable one to one solution bifurcates to a stable alternating solution, and then, the solution becomes stable blocking solution if T is too small. Physiologically speaking, the blocking phenomenon is different form alternans; however, they are both alternating solutions in the bifurcation analysis in my research. The only difference between them happens in the action potential duration (APD) restitution curves. In the red branch of Fig 5.8, before APD passes the minimum value as T decreases, it is an alternating solution; after APD passes the minimum value, the solution becomes a blocking solution. In the following figures, two solutions are differentiated in the same way. There is another period-doubling bifurcation, Label 4, occurring in the new branch, which happens in a lot of parameter sets in different subfamilies; however, it always happens after the blocking time so it is physiologically meaningless.

There are two distinctive representatives in F2, and they are in Fig. 5.9 and Fig. 5.10.
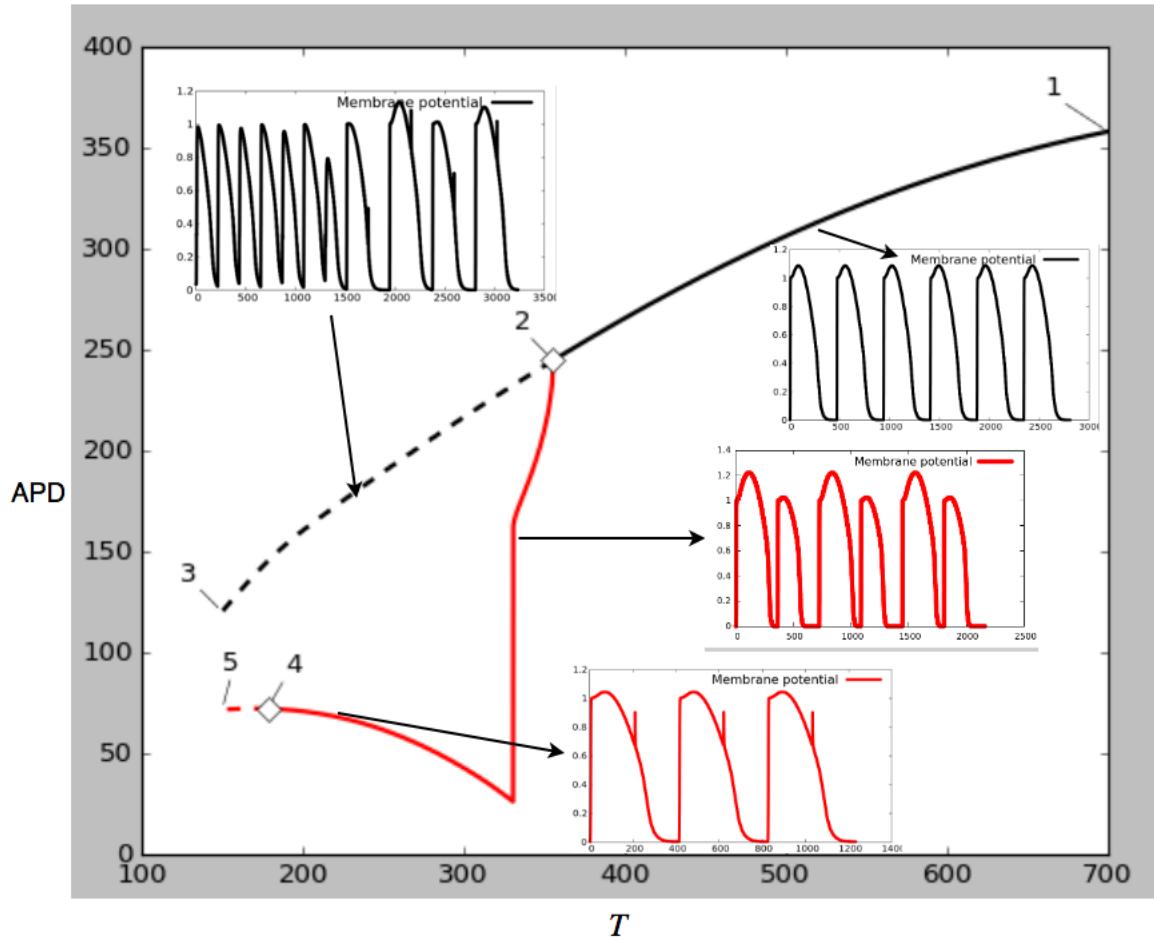
Figure 5.8: Continuation in T of one parameter set in F1. The interval $150\text{ms} \leq T \leq 700\text{ms}$ is considered physiologically meaningful. The black line is the equilibria in the main branch, and the red line represents the equilibria of the switched branch where the solid line represents the stable solution, and the dashed line indicates the unstable solution. Label 1 denotes the beginning of the continuation; label 2 is the period-doubling bifurcation; label 3 and label 5 are the ens of the continuation; label 4 is the period-doubling bifurcation in the switched branch.
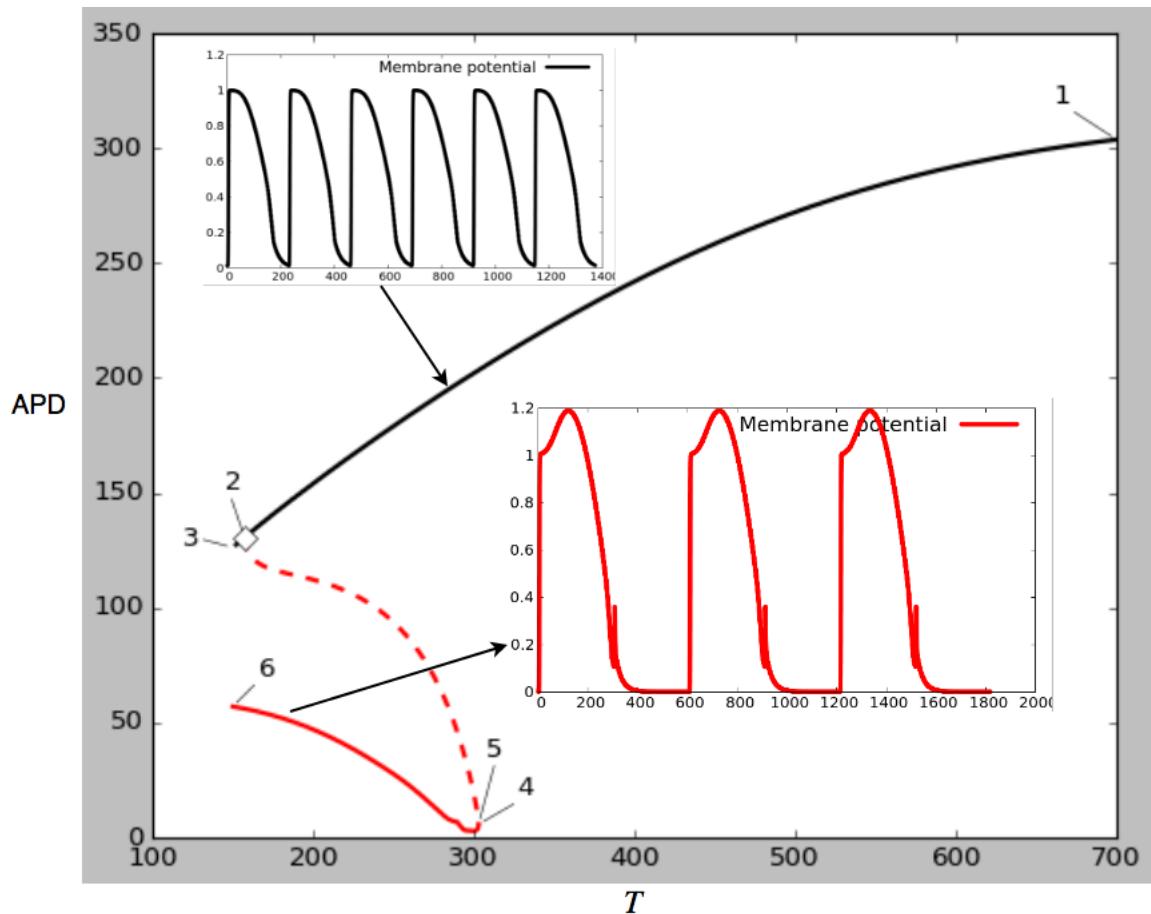
Figure 5.9: Continuation in T of one parameter set in F2, part 1. Label 1 shows the beginning of the continuation; label 2 is the period-doubling bifurcation; label 3 and label 6 are the ends of the continuation; label 4 and label 5 are the decreasing fold bifurcations in the switched branch.
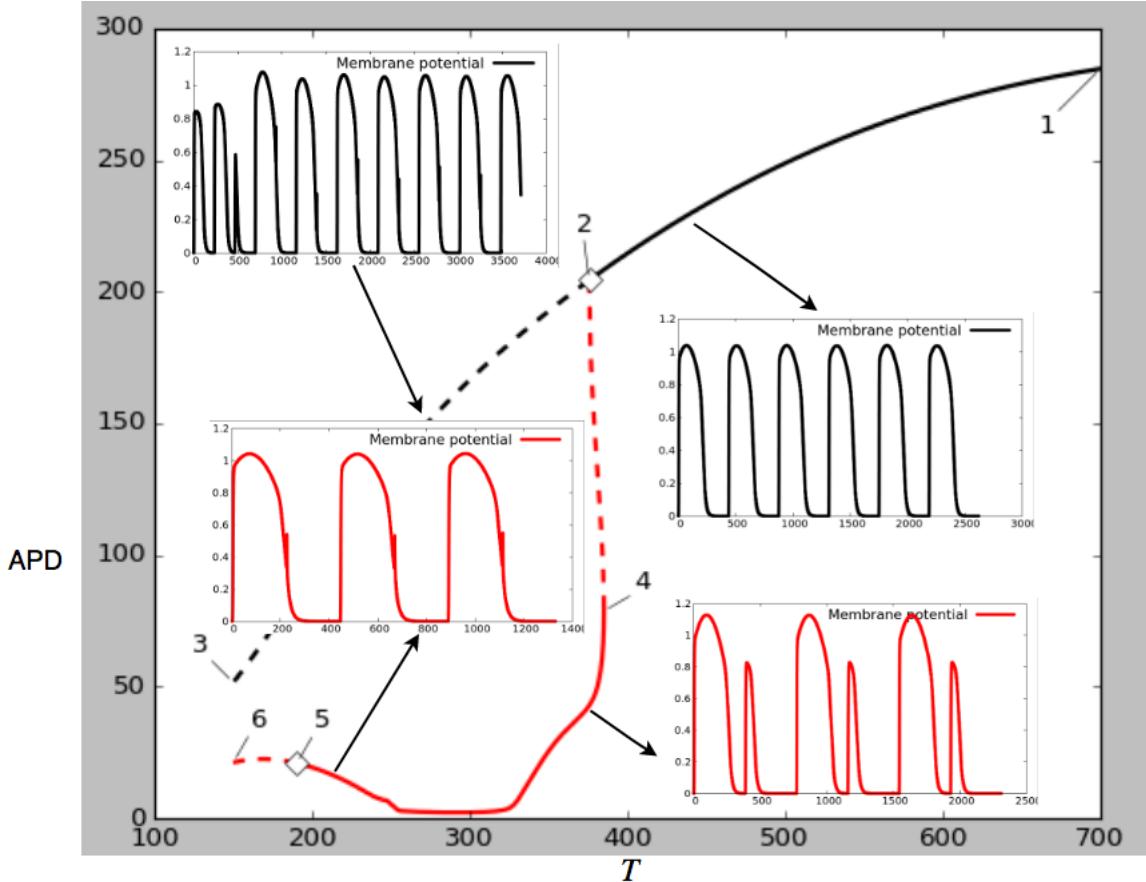
Figure 5.10: Continuation in T of one parameter set in F2, part 2. Label 1 expresses the beginning of the continuation; label 2 is the period-doubling bifurcation; label 3 and label 6 are the ends of the continuation; label 4 and label 5 show the decreasing fold bifurcation and the period-doubling bifurcation in the switched branch.

In Fig. 5.9, if the first period-doubling corresponds to a small value of T. Here, the stable one to one solution bifurcates to an unstable alternating solution shown as the red dashed line that can converge to the stable one to one solution or to the blocking solution when perturbed. We call this behavior bistability that will be discussed in the next section too. After the decreasing fold bifurcation, the unstable alternating bifurcates to a stable blocking solution. There are two labels showing the decreasing fold bifurcations because of numerical error that makes AUTO identify one bifurcation as two extremely close bifurcation points.
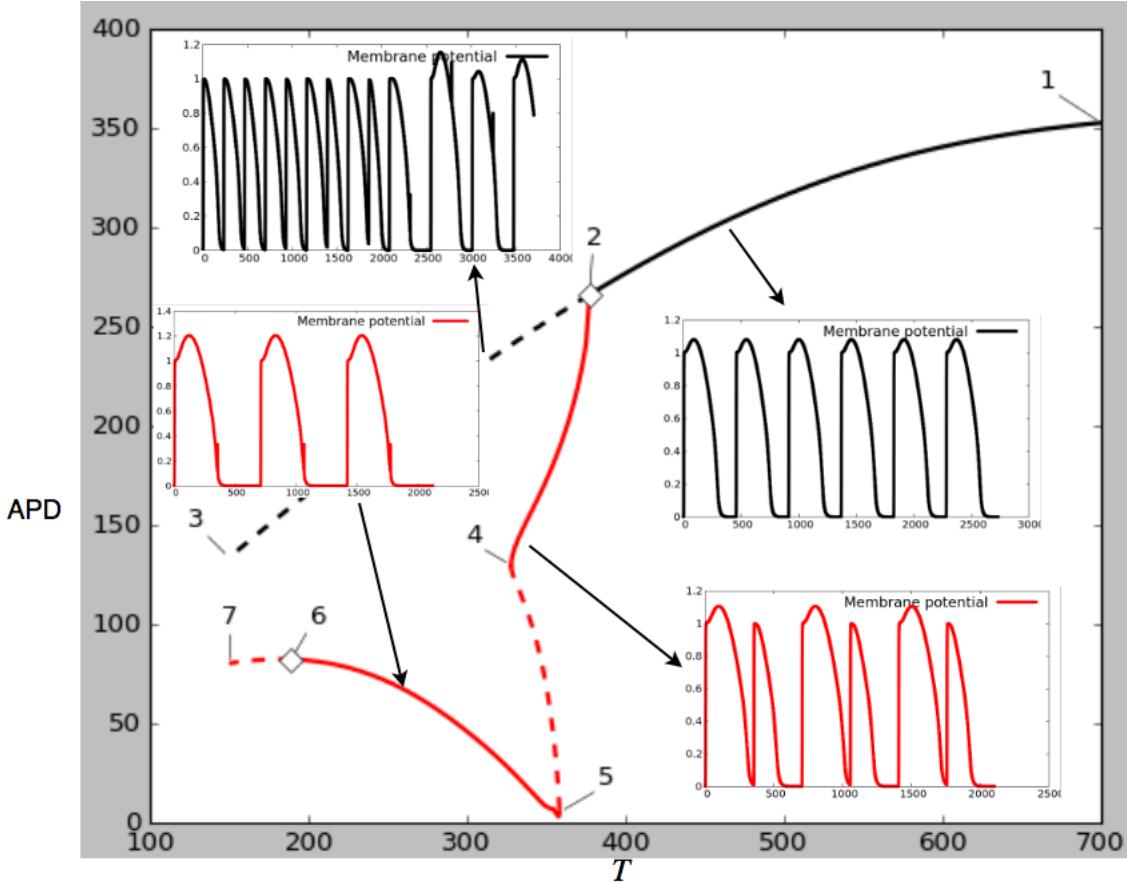
Figure 5.11: Continuation in T of one parameter set in F3. Label 1 is the beginning of the continuation; label 2 shows the period-doubling bifurcation; label 3 and label 7 are the ends of the continuation; label 4 and label 5 are the increasing fold bifurcation and the decreasing fold bifurcation in the switched branch; label 6 is the period-doubling bifurcation in that branch.

In Fig. 5.10, if the first period-doubling occurs when T is large, the stable one to one solution bifurcates to an unstable alternating solution shown as the red dashed line that can converge to stable one to one solution or stable alternating solution when perturbed, which is also bistability. As T decreases again, the unstable solution becomes a stable alternating solution, then a stable blocking solution.

In Fig. 5.11, after switching branches at the period-doubling bifurcation, the solution bifurcates to a stable alternating solution; then it becomes an unstable alternating solution that can converge to a stable alternating solution or a stable blocking solution, which
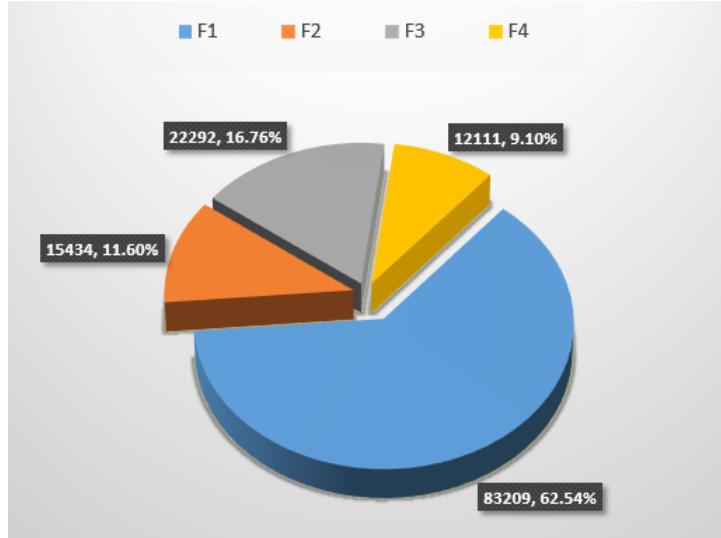
Figure 5.12: Percentage and the number of four subfamilies The total number is 133,046. The blue part is F1, the orange one is F2, the gray indicates F3, and the yellow part is F4.

still depends on the perturbation in this case. After the decreasing fold bifurcation, the solution turns into a stable blocking solution.

F4 includes other parameter sets, for instance , those that have too many misidentified bifurcation points on the branches or have convergence problems and so on. The percentage of these four subfamilies are in Fig 5.12

5.3 Similarities and differences in four subfamilies

By showing the properties of F1, F2 and F3 types of bifurcation diagrams, we can conclude that all of the 133,046 plots of the preliminary sets in PF2 fall into one of those four categories. We process the all sets in search of global, statistically relevant similarities and differences among F1, F2 and F3 regarding the physiological behaviors.

The first global difference among those subfamilies likely happens in the first period-doubling bifurcation namely the appearance of alternans. According to Fig. 5.13, F1 and F3 have the similar distributions of the period-doubling bifurcations; however, F2 has a
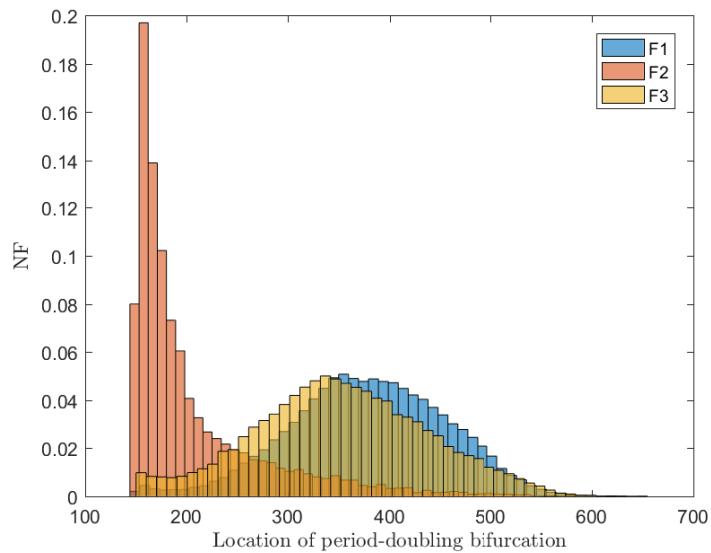
Figure 5.13: Distributions of the period-doubling bifurcation sorted by subfamilies.

The normalized frequencies of the period-doubling bifurcation values for the analyzed 133,046

parameter sets, with F1 in blue, F2 in orange and F3 in yellow. Average and standard deviation

are ($\mu = 378.42, \sigma = 76.45$) for F1 and($\mu = 206.12, \sigma = 68.70$) for F2 and ($\mu = 352.79, \sigma = 85.13$) for F3.
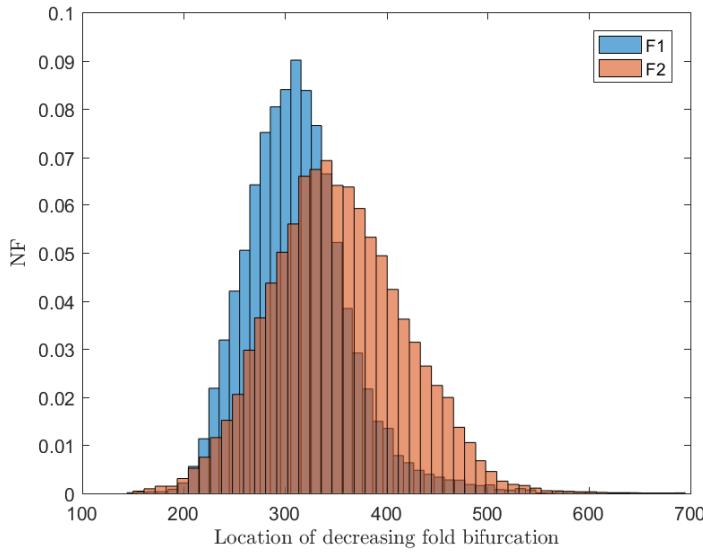
Figure 5.14: Distributions of the decreasing fold bifurcation sorted by subfamilies. The normalized frequencies of the decreasing fold bifurcation values for the analyzed 133,046 parameter sets, with F2 in blue, F3 in orange. Average and standard deviation are ($\mu = 312.37, \sigma = 51.71$) for F2 and($\mu = 352.04, \sigma = 65.25$) for F3.

distinctively different distribution, and most period-doubling bifurcation values in F2 are smaller than those in F1 and F3. Physiologically, the ventricular alternans happens at a slow pacing frequency in F1 and F3 but arrives at a high-speed pacing frequency in F2.

To know when the stable one to one solution becomes sensitive in F2 and F3, we compare the distributions of the decreasing fold bifurcation in F2 and F3, which results in the appearance of bistability. When bistability occurs, if we give a finite decimal perturbation, the stable one to one solution will converge to itself; if we give a large perturbation, the stable one to one solution will jump to a stable alternating solution or stable blocking solution. According to Fig. 5.14, the distributions of the decreasing fold bifurcation are similar in F2 and F3; therefore we can conclude that the bistability of F2 and F3 happens at a similar pacing frequency.

We would like to know how long the bistability exists until the period-doubling bifurcation occurs. Fig. 5.15 shows that the bistability in F2 lasts much longer than that
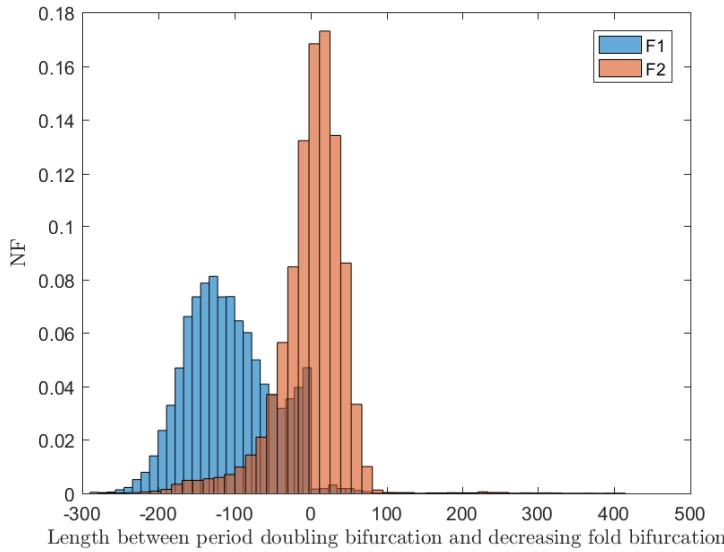
Figure 5.15: Distributions of the difference between the decreasing fold bifurcation and the period doubling bifurcation with respect to T sorted by subfamilies. The normalized frequencies of the distances between two bifurcation points for the analyzed 133,046 parameter sets, with F2 in blue, F3 in orange. Average and standard deviation are ($\mu = -106.25, \sigma = 56.95$) for F2 and ($\mu = 0.74, \sigma = 44.40$) for F3.

in F3 because the absolute mean of the distance between the decreasing fold bifurcation and the period-doubling bifurcation in F2 is much larger than the absolute mean of the distance in F3.

5.4 Partitioning and distributions of parameters

Besides responses (APDs) to the continuously increasing pacing frequency, we would like to know three subfamily partition showing that some normalized frequencies of parameter values exhibit significant differences for F1, F2 and F3. The rationale for this analysis is to determine the existence of specific parameters which have a predominant influence in causing the appearance of one subfamily of plots rather than another. In order to objectively assess these differences, we now compute the square root of the information
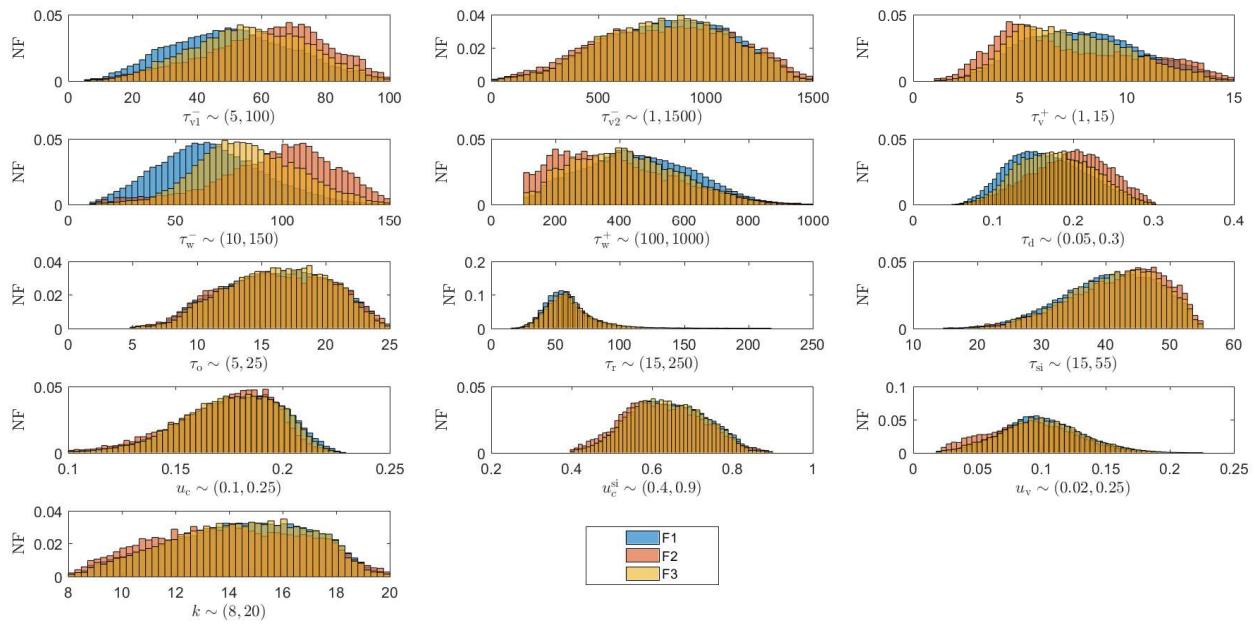
Figure 5.16: Normalized frequencies of thirteen parameters values by subfamilies. Blue bars are for F1, orange ones for F2 and yellow bars for F3. The total number of bins is 50, within the intervals of physiological validity indicated in Table. 2.1

radius (also known as the Jensen-Shannon divergence) among the histograms for each parameter i labeled g_j^i for F1, h_j^i for F2 and k_j^i for F3 with $j = 1, ..., nb$ bins. The following Eq.(5.2) shows how to compute Jensen-Shannon divergence between F1 and F2 as an example:

$$d_{IR}^i = \sqrt{\sum_{j=1}^{j=nb} [\frac{1}{2}(g_j^i log_2 g_j^i + h_j^i log_2 h_j^i) - m_j^i log_2 m_j^i]}$$
$$\text{with } m_j^i = \frac{1}{2}(g_j^i + h_j^i)$$
$$\sum_{j=1}^{j=nb} g_j^i = 1 \text{ and } \sum_{j=1}^{j=nb} h_j^i = 1 \tag{5.2}$$

which is a proper metric for the similarity of discrete probability distributions. Note that for empty bins, one defines $0 \ log_2 0 \equiv 0$. Identical distributions have $d_{IR} = 0$, whereas maximal dissimilarity is indicated by $d_{IR} = 1$.[14] The Jensen-Shannon divergences among F1, F2 and F3 are in Table. 5.2.

According to Table. 5.2, the five largest dissimilarities among the frequency distributions in Fig. 5.16 of three subfamilies are found for the same parameters τ_w^-, τ_{v1}^-, τ_d, τ_v^+ and τ_w^+, even though the orders of the magnitude of the dissimilarities are a little different, for example, τ_{v1}^- is that parameter showing the second large dissimilarity between F2 and F3 but ranks the fourth in the dissimilarity between F1 and F2, and the fifth in the dissimilarity between F1 and F3.

If a parameter set that belonging to PF2 has large values for τ_w^-, τ_{v1}^-, τ_d and small values for τ_v^+, τ_w^+, we can likely identify this parameter set as belonging to F1 according to Fig. 5.16. τ_w^- should have the most information on the classification because Jensen-Shannon divergences (d_{IR} of τ_w^- among three subfamilies are the largest).

	τ_{w}^{-}	τ_{v1}^{-}	τ_{d}	τ_{v}^{+}	τ_{w}^{+}	u_{v}	u_{c}
d_{IR} between F1 and F2	0.4714	0.2452	0.2425	0.2004	0.1993	0.108	0.098
d_{IR} between F1 and F3	0.3064	0.138	0.1067	0.0924	0.0953	0.0699	0.0359
d_{IR} between F2 and F3	0.2763	0.1419	0.1649	0.1824	0.1327	0.1241	0.0895
	τ_{si}	k	$u_{\mathrm{c}}^{\mathrm{si}}$	τ_{v2}^{-}	τ_{o}	τ_{r}	
d_{IR} between F1 and F2	0.0896	0.0821	0.0801	0.0689	0.0404	0.0223	
d_{IR} between F1 and F3	0.0486	0.0326	0.0412	0.0337	0.0445	0.0188	
d_{IR} between F2 and F3	0.0694	0.0904	0.0825	0.0756	0.067	0.0208	

Largest	Second large	Third large	Fourth large	Firth large

Table 5.2: Jensen-Shannon divergences (d_{IR}) among three subfamilies. The number in the grid shows the JensenShannon divergence between two distributions of two subfamilies where d_{IR} is from 0 to 1. The red grid shows the largest difference between two distributions, the blue grid is the second large difference, the yellow one represents the third large radius, the green one indicates the fourth large one and the orange one is the fifth large difference.

5.5 Identification of special points by parameters

In the previous section, according to some parameters or their combinations, we can determine what subfamily a parameter set in PF2 likely belongs to. Furthermore, we have introduced the special points like the period-doubling bifurcation that shows the presence and absence of alternans and the decreasing fold bifurcation that indicates the onset of bistability. Are there any relations between the parameters and the locations of the bifurcations in each subfamily? If we can find such relations, are the relations the same in three subfamilies?

In F1, the only special point is the period-doubling bifurcation showing the appearance of alternans.

Fig. 5.17 shows the relations between the twelve parameters and the location of alternans appearing. After magnifying each plot individually, we found τ_{r} and τ_{w}^{-} including
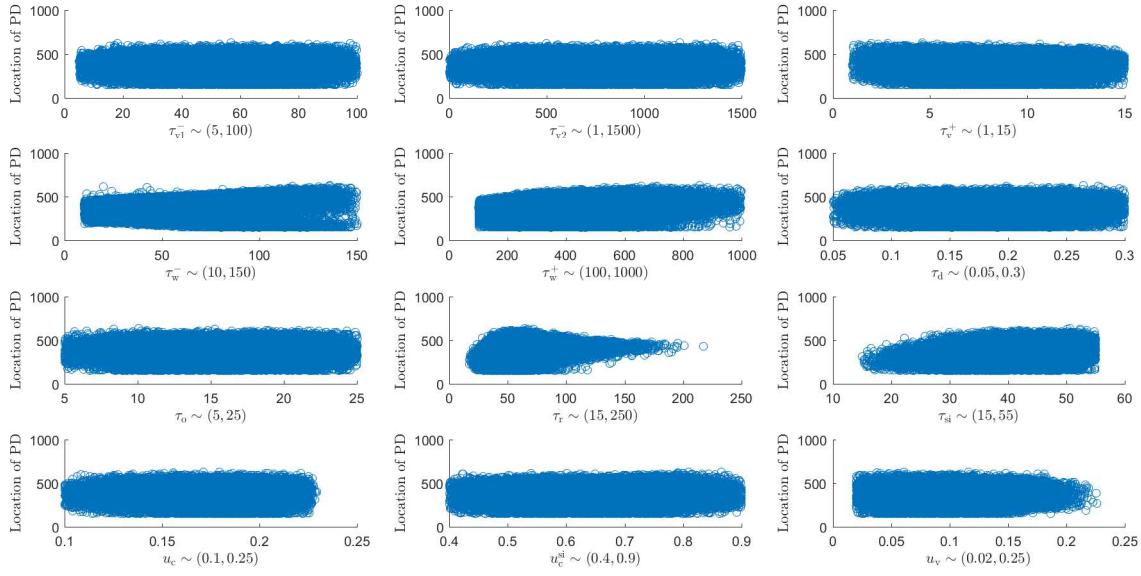
Figure 5.17: Scatter plots of twelve parameters VS the location of the period-doubing bifurcation in F1. In F1, the scatter plots of twelve parameters VS the location of the period-doubing bifurcation where x-axes are parameters and y-axes are the cycle length. The total number is 83,209, and the values shown in the curved bracket are the intervals.
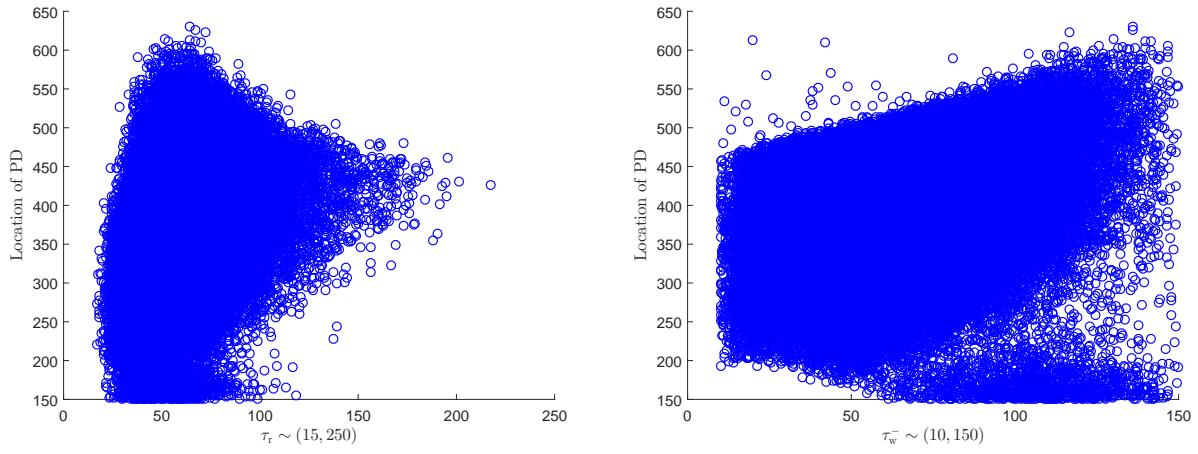
Figure 5.18: Scatter plots of τ_r and τ_w^- VS the location of the period-doubing bifurcation. The first plot is τ_r VS the cycle length where the period-doubing bifurcation appears, and the second plot is τ_w^- VS the cycle length at which the period-doubing bifurcation occurs. The number of total points is 83,209.
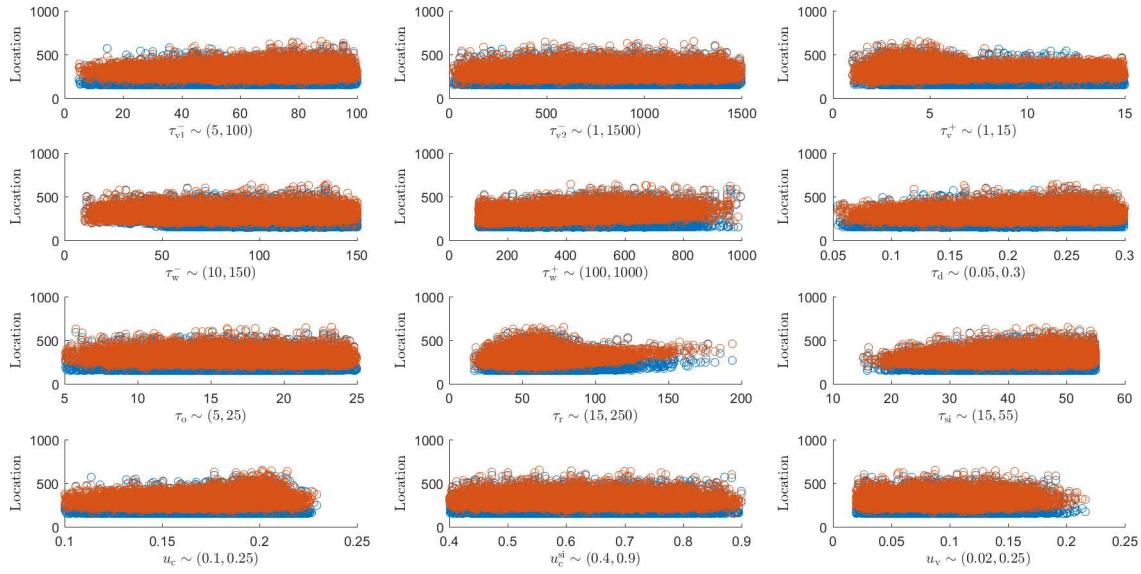
Figure 5.19: Scatter plots of twelve parameters VS the location of the period-doubing bifurcation and the decreasing fold bifurcation in F2. In F2, the scatter plots of twelve parameters VS the cycle length at which the period-doubing bifurcation (blue circle) and the decreasing fold bifurcation (red circle) appear. The total number is 15,434.

some information related to the period-doubling bifurcation. In the first figure of Fig. 5.18, we can see the range of the period-doubling bifurcation is decreasing from (150,650) to (400,450) as the value of τ_r increases. In the second graph of Fig. 5.18, it shows the opposite trend when the value of τ_w^- increases, the interval of the period-doubling bifurcation becomes larger.

In F2, there are two special points where one is the period-doubling bifurcation showing the occurrence of alternans, and the other one is the decreasing fold bifurcation that indicates the appearance of bistability.

Fig. 5.19 shows the relations between twelve parameters and two special points; τ_r is still a parameter that controls the intervals of those two particular points, and the more interesting result happens in τ_w^+. In Fig. 5.20, there is a positive linear relation between τ_w^+ and the location of the decreasing fold bifurcation but not the period-doubling
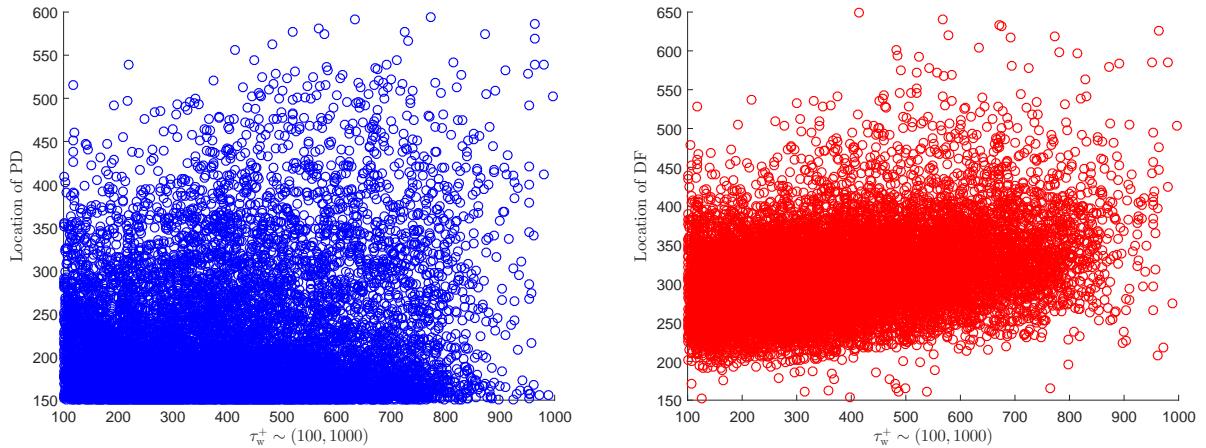
Figure 5.20: Scatter plots of τ_w^+ VS the location of two special bifurcation points in F2. The first plot is τ_w^+ VS the location of the period-doubing bifurcation and the second plot is τ_w^+ VS that of the decreasing fold bifurcation. The number of total points is 15,434.

bifurcation. τ_w^+ is related to the speed of Ca^{2+} entering the membrane, and bistability appears at a relatively slow pacing frequency when τ_w^+ is large and vice versa.

After observing and magnifying the figures in Fig. 5.21 individually, we can tell τ_r and τ_{si} control the ranges of special bifurcation points. Furthermore, there is a positive linear relation between τ_w^- and the location of the decreasing fold bifurcation shown in the second figure of Fig. 5.22; as for the first graph of Fig. 5.22, we can hardly tell the relation between τ_w^- and the location of the period-doubling bifurcation.

In conclusion, after partitioning the parameter sets belonging to PF2 to three sub-families, some parameters like τ_w^-, τ_w^+ and τ_r significantly include the extra information showing the relations with the appearance of alternans and the presence of bistability.
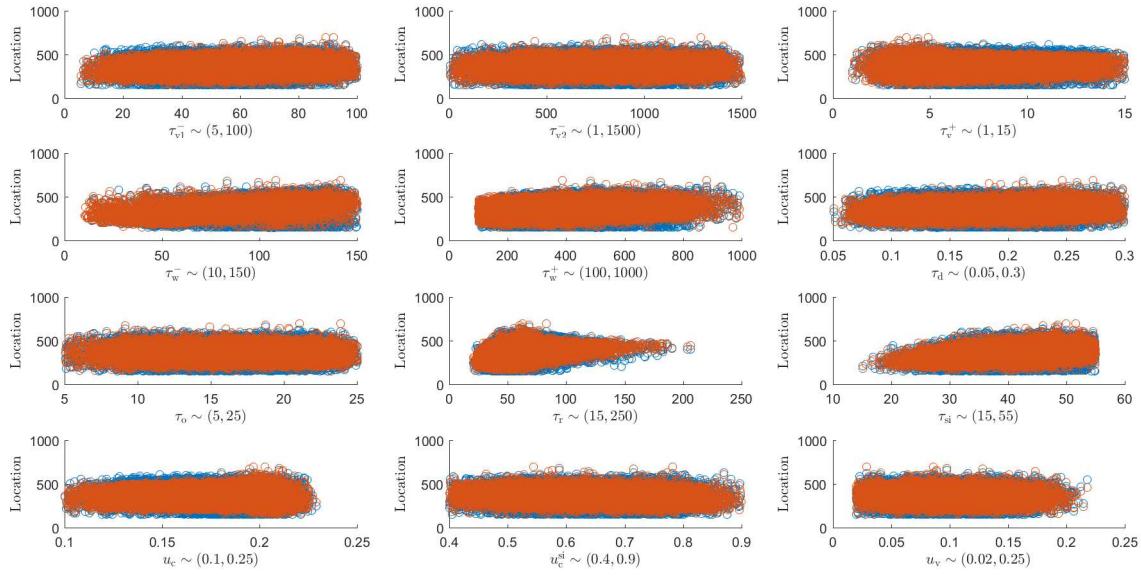
Figure 5.21: Scatter plots of twelve parameters VS the location of the period-doubing bifurcation and the decreasing fold bifurcation in F3. In F3, the scatter plots of twelve parameters VS the cycle length at which the period-doubing bifurcation (blue circle) and the decreasing fold bifurcation (red circle) appear. The total number is 22,292.
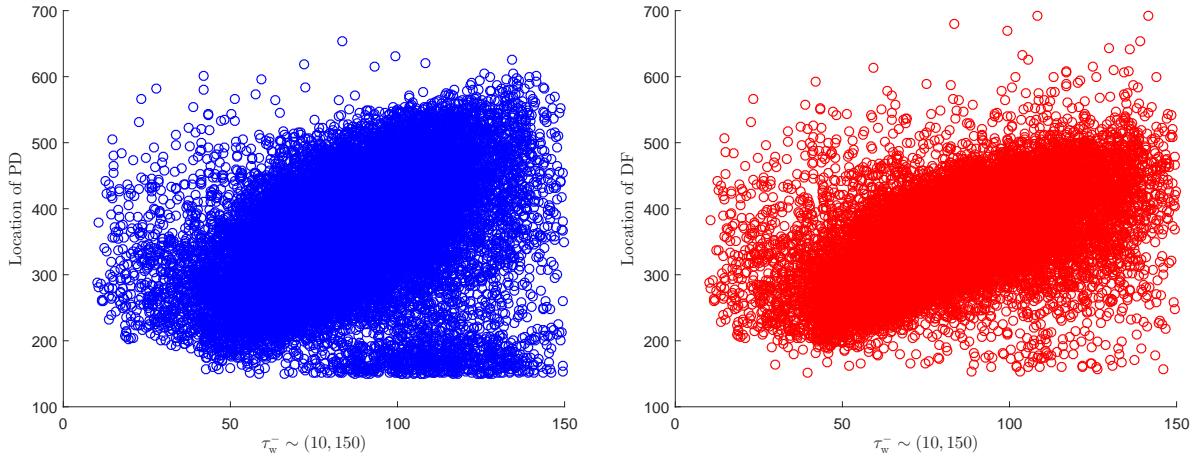
Figure 5.22: Scatter plots of τ_w^- VS the location of two special bifurcation points in F3. The first plot is τ_w^- VS the cycle length at which the period-doubing bifurcation occurs and the second plot is τ_w^- VS the cycle length at which the decreasing fold bifurcation appears. The number of total points is 22,292.

Chapter 6

Discussion

6.1 Innovations

We have illustrated how bifurcation diagrams of the F-K model change as one control parameter T varies.

Compared with limit point diagrams, drawn by time-stepping integration, a model for a finite number of values of T[16] [9], our bifurcation diagrams can accurately indicate not only the special points like the period-doubling bifurcations and the decreasing fold bifurcations but also the unstable equilibria. When the pacing frequency increases, the response of the ventricular cell in the F-K model is not as simple as being understood so far. For example, the stable one to one solution can jump to a stable alternating solution or even a stable blocking solution, depending on the physiologically meaningful combination of parameters and the perturbation given to the system. Compared with the papers that do not draw the detailed bifurcation graphs, our research can find some complex behaviors such as the bistability.

Most papers about phenomenological models of ventricular cells are based on choosing some specific and optimized combinations of parameters to show the relation between the APD restitution curves and the increasing pacing frequency. Different results have been

published such as: Guevara *et al.* (1984) [16] has found alternans existing in some param-
eter sets; Cherry *et al.* (2004) [4] have shown the blocking phenomenon occurs in some
parameter sets when the pacing is fast; all these results are based on specific parameter
sets. Why do some parameter sets have alternans but some do not? What parameters
play the leading roles to control the cycle length at which the blocking phenomenon or
alternans occur? What information is hidden behind the parameters resulting in the
significantly different behaviors? There is not even one paper that systematically explore
the relation between parameter effects and the behaviors of electric activity in ventricular
cells. In my research, we have have searched the parameter space to obtain physiolog-
ically reasonable combinations of parameters that can simulate almost all the possible
responses in the F-K model. After drawing the bifurcation plots, we can see what qual-
itative behaviors the F-K model can have when the pacing frequency increases. After
partitioning the parameter sets in PF2, with only one period-doubling bifurcation, into
four subfamilies, we have found significant information. For example, τ_w^- can statistically
identify the different qualitative behaviors among F1, F2 and F3; for instance, if there
is one parameter set where τ_w^- is between 133ms and 135ms, we can say there is 71.24%
likelihood that this parameter set belongs to F2, 5.33% chance that the parameter set be-
longs to F1 and 23.43% probability that belongs to F3. τ_r τ_w^- are related to the ranges of
alternans and bistability, and so on. It is common to compare different phenomenological
ventricular cell models (see e.g. [9] [2])with some specific parameter sets; however, these
models are created based on the ion currents and storage between the cells and the body
liquid, and most of them have similar or even some identical parameters. The number of
models is large but the number of parameters is relative small and able to be analyzed.
Rather than comparing different phenomenological ventricular cell models, we explore
one of them to obtain the significant and distinctive information that each parameter
includes and establish the relations between parameters and responses. For example, in
F3, we can conclude that when the value of τ_w^- is lager, the bistability appears earlier as

the pacing frequency increases.

Frascoli *et al.* (2011)[14] first introduced metabifurcation analysis to discover robust correlations between physiological parameters of a model of electric activity in the cortex and its dynamical features. In my research, we have taken the idea of the metabifurcation analysis and implemented it for the F-K model.

6.2 Discussion of the results

It is important to appreciate the generality and simplicity of the methods we have used here. We have chosen the meaningful parameters for the bifurcation analysis and have then classified parameter sets into five parent families based on the number of the period-doubling bifurcations since the period-doubling bifurcation is the appearance and the disappearance of alternans. Is the classification in parent families reasonable? Physiologically speaking, some second or third period doubling bifurcation happen at the pacing frequency that is faster than the blocking pacing frequency. If we do not count the period-doubling bifurcations happening when the pacing is faster than blocking frequency, we can make the classification in parent families more precise. However, there are two difficulties: The first one is the blocking phenomenon happens at different pacing frequencies among those 270 thousand physiologically meaningful parameter sets; some occur after the first period-doubling bifurcation, and some happen after the second period doubling bifurcation. Therefore, we hardly allocate it. Second, the convergence problem makes the continuation fail after switching branches at the period-doubling bifurcations, which make the first problem more difficult to find the the blocking cycle length for each parameter set.

Due to the aforementioned difficulties, the classification is reasonable in five parent families based on the number of the period-doubling bifurcations. In terms of the classification for PF2, we have classified PF2 into four subfamilies based on the three probable

dynamical patterns. However, more sophisticated criteria for labeling the resulting bifur-
cation plots could be envisaged. For example, subfamilies might have been categorized
by adding more other types of bifurcations, it will result in more families classified; nev-
ertheless, the physiological meaning has to be considered; some parameter sets have a
period-doubling bifurcation that happens in the branch after the blocking period, so it
is not wise to set that as a new criterion. Across a large number of parameter sets, we
have listed and identified most possible diagrams in PF2. A small number of bifurcation
graphs still cannot be classified, and most of them in F4 have the convergence problem
because the two bifurcation points are identified at the same forcing period.

My research can offer a guidance by implementing the dynamical approach. A PCA
on the 1,525,833 analyzed parameter sets turns out to be largely useless. It is also true if
we employ the PCA after dividing the parameter sets belonging to PF2 into subfamilies:
the first three principal components, with the largest factor scores, account for about 41%
of the total variance in F1, F2 and up to 34% in F3. Again, the valuable information on
parameter relations still can not be gleaned by implementing the PCA process in those
subfamilies. If we compare Fig. 5.2 with the clear separation among distributions of
$\tau_{\mathrm{w}}-$ in three families in Fig. 5.16, we can appreciate the strength of the metabifurcation
analysis to tease out hidden correlations in the F-K model.

$\tau_{\mathrm{w}}-$ plays the leading role of partitioning in terms of three subfamilies. The reason
is that the dynamical patterns of three subfamilies basically indicate the different onsets
of alternans, and the appearance of alternans is closely related to diastolic interval(DI)
and recovering time. When the value $\tau_{\mathrm{w}}-$ is large, slow gating variable w needs shorter
time to recover because the effect of reactivation of slow inward currents is not strong,
and a shorter DI needed to ensure the normal behavior; therefore, when we decrease the
forcing period T, alternans appears at a relatively faster pacing frequency compared with
the small value of $\tau_{\mathrm{w}}-$. We can verify this conclusion by comparing Fig. 5.16 and Fig.
5.13.

Phenomenological ventricular cell models have been analyzed in some published papers. By comparing the results that we have obtained, we can not only establish the confidence in my research but also tell the similarities and differences between both. Figure 3 in the paper[37] shows the three typical limit point diagrams between in vivo and in silico based on the OHaraRudy model at a cell level; normal, eye type alternans and fork type alternans, in the OHaraRudy model, correspond to PF1, PF2 and PF3 in my research. Those three parent families occupy more than 90%. Furthermore, Figure 2 of the paper[15] illustrates two different limit point graphs, in rabbit ventricular cells, that are related to PF1 and PF2 accounting for 70%. Because those papers implement the limit point graphs to capture some dynamical features with some specific parameter sets, we can only see the most common results like graphs in PF1, PF2 and PF3. However, besides those common dynamical behaviors, there are some more interesting results. For example, Qu (2010) shows one more exciting bifurcation diagram of one cardiac model at the cellular level when the control parameter CL decreases; in Figure 3(C) of the paper[27], a one to one solution becomes a two to two alternating solution, then it becomes a two to one blocking solution and more and more complicated to chaos. We can see there is an jump between the two to two alternating solution and the one to two blocking solution. F3 also shows the similar result; in Fig. 5.11, we can see the alternating solution becomes blocking solution with a jump after Label 4 as T decreases. F3 only fill around 16% of PF2 and less than 8% of the whole physiological meaningful parameter sets. Most phenomenological ventricular cell models are created based on the similar physiological features with more or fewer parameters and variables; therefore, they will have the similar behaviors like the F-K model, the OHaraRudy model and so on. The results from other papers can only tell us the tip of the iceberg such as the graphs belonging to PF1, PF2, PF3 and F3. After doing the metabifurcation analysis, we can see almost all kinds of results like F1 and F2. Unfortunately, we have not done the sub-classification in PF3 and PF4 because the complex behaviors after switching
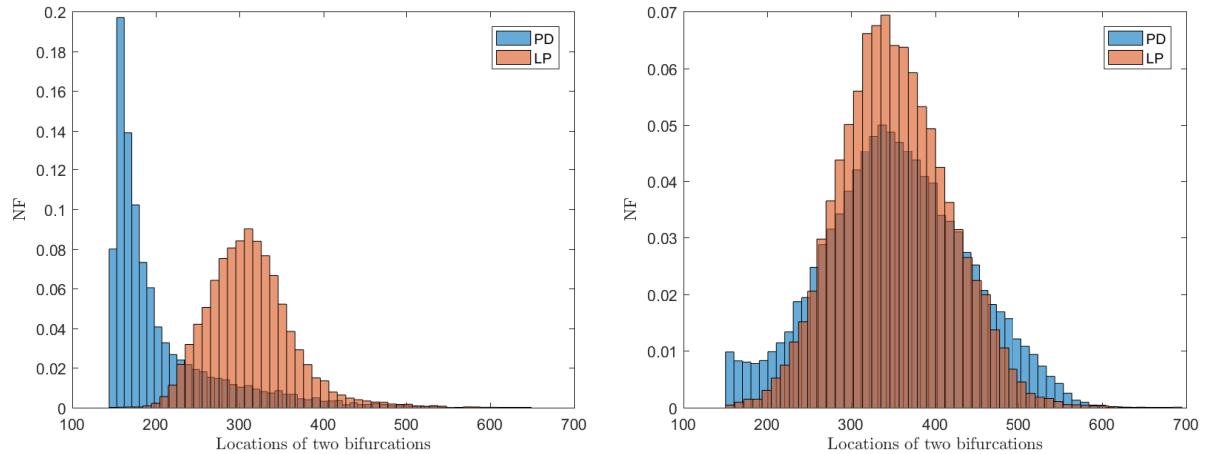
Figure 6.1: The distributions of the period-doubling bifurcation and the decreasing fold bifurcation in F2 and F3 The first plot shows two distributions of two bifurcations in F2 where PD is the period-doubling bifurcation and LP is the decreasing fold bifurcation, the second plot shows two distributions of two bifurcations in F3

branches at period-doubling bifurcations.

Some interesting and open questions also exist in the results. According to Fig. 6.1, F2 and F3 have the significantly different distributions of the period-doubling bifurcation; however, they have the similar distributions of the decreasing fold bifurcations. Are there some relations between two subfamilies or two bifurcations? In F2, after the bistability occurs, the behavior is sensitive to the perturbation so the stable one to one solution can quickly jump to the stable alternating solution. Therefore, the bistability phenomenon might correspond to the onset of alternans. In F3, both distributions are similar; it also indicates that bistability phenomenon can be considered as the beginning of alternans in some degree. If that is true, alternans occurs at the decreasing fold bifurcation rather than the period-doubling bifurcation, which has not been discovered before, and the first period-doubling bifurcation has been defined as the onset of alternans in the papers we have learned on phenomenological ventricular cell models so far.

After partitioning the parameter sets in PF2 into four subfamilies, we have listed the relations between parameters and the onsets of bistability and alternans. There is

another essential phenomenon that indicates the important moment, which is blocking phenomenon . We would like to know how the blocking phenomenon related to some parameters in some families like the linear relation between τ_w^- and the bistability in F3? In some bifurcation diagrams, the decreasing fold bifurcation can indicate the blocking phenomenon; however, in most bifurcation diagrams, there is not a bifurcation label can indicate the blocking phenomenon. According to the representatives of bifurcation diagram from Fig. 5.8 to 5.11, when the value of APD passes the minimum value in branches, we call that forcing period as the onset of the blocking phenomenon. One way is to add or rewrite some code in AUTO to allocate the cycle length of the onset of the blocking phenomenon; the other way is to decompose the output files from AUTO to write the shell and python scripts to find that minimum value in T as the cycle length of the block phenomenon.

6.3   Future work

1. The great hurdle is represented by the computational limitation: it is still unfeasible to process all sets one by one and see all bifurcation diagrams, which will help us increase our knowledge about the types of dynamics the F-K model can produce. Maybe we can implement this process in GPU rather than CPU.

2. In the research, we implement the time-step integration of the F-K model to obtain a Poincaré map. Even the error is 10^{-14} in each time step and each time step is 0.05ms, the accumulated error over one period can still cause some convergence problems. Rather than integrate the OEDs in the F-K model, we can use a discrete map, which will be computationally cheap and accurate. However, the discrete map[26] is not accurate as the Poincaré map, and there will be some problems when we implement that to replace the integration of the F-K model.

3. The horizontal comparison among different models with using metabifurcation

analysis can be considered. The reason is that different phenomenological models of ventricular cells are based on both the concentration of ions between cell sap and body sap and the change of currents. Therefore, most parameters have the similar meaning among these models. After comparing different models, the results will be more reliable. One of the difficulties will be in the comparison, in some model, one parameter can represent one feature; in another model, two, three or even more parameters can express the same property; how to combine the parameters to let them comparable regarding the same property?

4. The F-K model can also be extended from the single cell level to the tissue level, which will result in solving the PDEs numerically. The computational time of the time-step integration in two or three dimensions will be exponentially longer. How to make the computational process efficient and the results reliable will be a big challenge. We have used AUTO to do the bifurcation analysis and draw the bifurcation diagram in the research; however, AUTO has not supported to solve PDEs numerically to do the bifurcation analysis yet, which means that we have to write our code to do the bifurcation analysis.

5. K-means clustering can be implemented to give another piece of information in the future research. Now, we know the distributions of parameters but we can not generate a sample parameter set in the given family. If we use the K-means clustering after the classification, we can parse the data and generate a physiologically meaningful parameter set in that given family.

Bibliography

[1] Jacob Benesty, Jingdong Chen, Yiteng Huang, and Israel Cohen. Pearson correlation coefficient. In *Noise reduction in speech processing*, pages 1–4. Springer, 2009.

[2] Alfonso Bueno-Orovio, Elizabeth M Cherry, and Flavio H Fenton. Minimal model for human ventricular action potentials in tissue. *Journal of theoretical biology*, 253(3):544–560, 2008.

[3] Darby I Cairns, Flavio H Fenton, and EM Cherry. Efficient parameterization of cardiac action potential models using a genetic algorithm. *Chaos: An Interdisciplinary Journal of Nonlinear Science*, 27(9):093922, 2017.

[4] Elizabeth M Cherry and Flavio H Fenton. Suppression of alternans and conduction blocks despite steep apd restitution: electrotonic, memory, and conduction velocity restitution effects. *American Journal of Physiology-Heart and Circulatory Physiology*, 286(6):H2332–H2341, 2004.

[5] RH Clayton, Olivier Bernus, EM Cherry, Hans Dierckx, FH Fenton, L Mirabella, AV Panfilov, Frank B Sachse, G Seemann, and H Zhang. Models of cardiac tissue electrophysiology: progress, challenges and open questions. *Progress in biophysics and molecular biology*, 104(1-3):22–48, 2011.

[6] Paul L DeVries and Javier E Hasbun. *A first course in computational physics*. Jones & Bartlett Publishers, 2011.

[7] Eusebius J Doedel, Alan R Champneys, F Dercole, TF Fairgrieve, A Yu, B Oldeman, RC Paffenroth, B Sandstede, XJ Wang, CH Zhang, et al. Auto-07p: Continuation and bifurcation software for ordinary differential equations. 2007.

[8] Joshua N Edwards and Lothar A Blatter. Cardiac alternans and intracellular calcium cycling. *Clinical and Experimental Pharmacology and Physiology*, 41(7):524–532, 2014.

[9] Mohamed M Elshrif and Elizabeth M Cherry. A quantitative comparison of the behavior of human ventricular cardiac electrophysiology models in tissue. *PloS one*, 9(1):e84401, 2014.

[10] Flavio Fenton and Alain Karma. Vortex dynamics in three-dimensional continuous myocardium with fiber rotation: Filament instability and fibrillation. *Chaos: An Interdisciplinary Journal of Nonlinear Science*, 8(1):20–47, 1998.

[11] Flavio H Fenton. *Theoretical investigation of spiral and scroll wave instabilities underlying cardiac fibrillation: a dissertation*. PhD thesis, Northeastern University, 1999.

[12] Richard FitzHugh. Impulses and physiological states in theoretical models of nerve membrane. *Biophysical journal*, 1(6):445–466, 1961.

[13] Jeffrey J Fox, Jennifer L McHarg, and Robert F Gilmour Jr. Ionic mechanism of electrical alternans. *American Journal of Physiology-Heart and Circulatory Physiology*, 282(2):H516–H530, 2002.

[14] Federico Frascoli, Lennaert Van Veen, Ingo Bojak, and David TJ Liley. Metabifurcation analysis of a mean field model of the cortex. *Physica D: Nonlinear Phenomena*, 240(11):949–962, 2011.

[15] Stephen Gaeta and David J Christini. Non-linear dynamics of cardiac alternans: subcellular to tissue-level mechanisms of arrhythmia. *Frontiers in physiology*, 3:157, 2012.

[16] MR Guevara, G Ward, A Shrier, and L Glass. Electrical alternans and period doubling bifurcations. *IEEE Comp Cardiol*, 562:167–170, 1984.

[17] Jun Han and Claudio Moraga. The influence of the sigmoid function parameters on the speed of backpropagation learning. In *International Workshop on Artificial Neural Networks*, pages 195–201. Springer, 1995.

[18] Alan L Hodgkin and Andrew F Huxley. A quantitative description of membrane current and its application to conduction and excitation in nerve. *The Journal of physiology*, 117(4):500–544, 1952.

[19] M Jayanthi and R Vinodha. Prolongation of interpeak latency of brainstem auditory evoked potential in hypothyroidism. *Int J Med Res Health Sci*, 5(3):22–27, 2016.

[20] James Kennedy. Particle swarm optimization. In *Encyclopedia of machine learning*, pages 760–766. Springer, 2011.

[21] "Dr. Michelle Khoo". "cardiac arrhythmia". *"http://www.khoocardiology.com/cardiology/conditions-we-treat/cardiac-arrhythmias"*.

[22] Aman Mahajan, Yohannes Shiferaw, Daisuke Sato, Ali Baher, Riccardo Olcese, Lai-Hua Xie, Ming-Jim Yang, Peng-Sheng Chen, Juan G Restrepo, Alain Karma, et al. A rabbit ventricular action potential model replicating cardiac dynamics at rapid heart rates. *Biophysical journal*, 94(2):392–410, 2008.

[23] Manoj Mali, Neha Goyal, and Himanshu Trivedi. Geometric methods in the theory of ordinary differential equations: A review.

[24] Sanjiv M Narayan. T-wave alternans and the susceptibility to ventricular arrhythmias. *Journal of the American College of Cardiology*, 47(2):269–281, 2006.

[25] Karl Pearson. Liii. on lines and planes of closest fit to systems of points in space. *The London, Edinburgh, and Dublin Philosophical Magazine and Journal of Science*, 2(11):559–572, 1901.

[26] Zhilin Qu, Yohannes Shiferaw, and James N Weiss. Nonlinear dynamics of cardiac excitation-contraction coupling: an iterated map study. *Physical Review E*, 75(1):011927, 2007.

[27] Zhilin Qu, Yuanfang Xie, Alan Garfinkel, and James N Weiss. T-wave alternans and arrhythmogenesis in cardiac diseases. *Frontiers in physiology*, 1:154, 2010.

[28] Thomas R Shannon, Fei Wang, José Puglisi, Christopher Weber, and Donald M Bers. A mathematical treatment of integrated ca dynamics within the ventricular myocyte. *Biophysical journal*, 87(5):3351–3371, 2004.

[29] PJA Shaw. Multivariate statistics for the environmental sciences, hod-der-arnold. Technical report, ISBN 0-340-80763-6.[page needed], 2003.

[30] Yuhui Shi and Russell Eberhart. A modified particle swarm optimizer. In *Evolutionary Computation Proceedings, 1998. IEEE World Congress on Computational Intelligence., The 1998 IEEE International Conference on*, pages 69–73. IEEE, 1998.

[31] Abraham Silberschatz, Peter Baer Galvin, and Greg Gagne. *Operating system concepts essentials*. John Wiley & Sons, Inc., 2014.

[32] David Sli, Endre; Mayers. *An Introduction to Numerical Analysis*. Cambridge University Press, 2003.

[33] Kristian Thygesen, Joseph S Alpert, Allan S Jaffe, Maarten L Simoons, Bernard R Chaitman, Harvey D White, Writing Group on behalf of the Joint

ESC/ACCF/AHA/WHF Task Force for the Universal Definition of Myocardial Infarction, Authors/Task Force Members Chairpersons, Kristian Thygesen, Joseph S Alpert, et al. Third universal definition of myocardial infarction. *European heart journal*, 33(20):2551–2567, 2012.

[34] EG Tolkacheva, DG Schaeffer, DJ Gauthier, and CC Mitchell. Analysis of the fenton–karma model through an approximation by a one-dimensional map. *Chaos: An Interdisciplinary Journal of Nonlinear Science*, 12(4):1034–1042, 2002.

[35] James N Weiss, Michael Nivala, Alan Garfinkel, and Zhilin Qu. Alternans and arrhythmias: from cell to heart. *Circulation research*, 108(1):98–112, 2011.

[36] Raimond L Winslow, Jeremy Rice, Saleet Jafri, Eduardo Marban, and Brian ORourke. Mechanisms of altered excitation-contraction coupling in canine tachycardia-induced heart failure, ii: model studies. *Circulation research*, 84(5):571–586, 1999.

[37] Xin Zhou, Alfonso Bueno-Orovio, Michele Orini, Ben Hanson, Martin Hayward, Peter Taggart, Pier D Lambiase, Kevin Burrage, and Blanca Rodriguez. In vivo and in silico investigation into mechanisms of frequency dependence of repolarization alternans in human ventricular cardiomyocytesnovelty and significance. *Circulation research*, 118(2):266–278, 2016.